UNIVERSITY OF GHANA, LEGON

COLLEGE OF BASIC AND APPLIED SCIENCES

CHARACTERIZATION OF WRF SIMULATED LOW-LEVEL JETS OVER SOUTHERN WEST AFRICA

BY

AMEYAW ODURO PRINCE

(10874887)

This thesis/dissertation is submitted to the University of Ghana, Legon in partial fulfillment of the requirement for the award of **MPHIL IN PHYSICS Degree**.

DEPARTMENT OF PHYSICS

December, 2022

DECLARATION

I hereby declare that this submission is my own work and that, to the best of my knowledge, it contains no material previously published by another person nor materials which has been accepted for the award of any other degree of the university, except where due acknowledgement has been made in the text.

…….. Date: 24 / 10 / 2023

AMEYAW ODURO PRINCE

(candidate:10874887)

…….. Date: 24 / 10 / 2023

(PROF. NANA AMA BROWNE KLUTSE)

(Principal Supervisor)

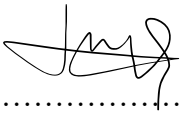

…….. Date: 24 / 10 / 2023

(DR. AZODA HUBERT KOFFI)

(Co-Supervisor)

DEDICATION

This research work is dedicated to my niece; Nana Ama Nhyira Amoyaw and my parents.

ACKNOWLEDGEMENT

The writing, computation and analysis of this research work was supported by Prof. Nana Ama Browne Klutse and Dr. Gandome Mayeul L. Davy Quenum. I would like to acknowledge the African Institute of Mathematical Sciences (AIMS, Ghana), for supporting this research financially through scholarship grants. The Center for High-Performance Computing (CHPC, Cape town, South Africa) also provided computing facilities for the study. I would also like to acknowledge the European Center for Medium-Range Weather Forecasts (ECMWF) and National Center for Environmental Prediction (NCEP), for providing operational analysis dataset and products.

TABLE OF CONTENT

LIST OF TABLES

LIST OF FIGURES

ABSTRACT

Low-level jets are mainly nocturnal phenomena with relatively strong horizontal winds in the lower section of the troposphere. The development and evolution of deep convection are linked to the low-level jets, which are vital for both horizontal and vertical fluxes of temperature and moisture. The focus of this study is to characterize low-level jets simulated with the WRF model in the planetary boundary layer (PBL) over southern West Africa. The simulation's forcing data were Global Forecast System datasets (GFS) and boundary conditions were specified in the WRF runs at 3-hourly temporal resolution. The performance of the simulation was tested with observational datasets from the European Center for Medium-range Weather Forecast (ECMWF). The study examined low-level jet characteristics such as frequency, intensity, height of occurrence, and direction of propagation. Three bioclimatic regions namely West Sudanian Savanna, Guinean, and Guineo-Congolian that can be found in southern West Africa were used as the basis for the analysis. The study employed a relative and absolute detection criteria for low-level jets which requires that the lowest maximum of a vertical wind speed profile in the lowest 1800 m of the atmosphere is at least 2 m/s and 25% stronger than the next minimum above. It was found that low-level jets are more frequent in the Guineo-Congolian than, West Sudanian Savanna and Guinean regions and about 90% occurring between the hours of 000 UTC and 060 UTC with south-westerlies dominating. The maximum average intensities of low-level jets in the Guineo-Congolian, West Sudanian Savanna and Guinean regions are 8.1 m/s, 12.9 m/s and 8.9 m/s respectively. Low-level jets observed do frequently occur between the height of 700 – 750 m above ground level, an average of 725 m. The study recommends more observational and modeling case

study on low-level jets over southern West Africa to emphasize conclusions made in the study.

CHAPTER ONE

INTRODUCTION

1.1 Background of Study

The atmosphere is a layer of gases, that surrounds the planet earth and is retained by earth's gravity. Temperature varies with height and has a complex profile that helps identify the atmospheric layers whereas atmospheric parameters such as pressure and density decrease with altitude. The troposphere is the lowest layer of the atmospheric layers, which rise on average to a height of roughly 13km from the surface of the earth. Due to surface heating, the height of the troposphere over a region changes over time. The planetary boundary layer (PBL), which rises from the earth's surface to a height of about 1.2 km, and the free atmosphere, which is located directly above it, make up the two main components of the troposphere (Slättberg, 2020). The free atmosphere and the earth's surface have a significant impact on the PBL. The PBL is influenced by surface heating, topography, frictional drag, evapotranspiration, and solar heating. The air just above the earth's surface is affected by solar heating and terrestrial cooling, leading to conditions of stability and instability within the PBL. Rapid vertical mixing caused by instability conditions redistributes mass, momentum, and heat. The mixing might be either mechanically or thermally caused (Carpman, 2011). As a result, a stable boundary layer forms near the surface, and the top part of the daytime mixed layer transforms into the residual layer within the PBL (Hu et al., 2013). According to the geostrophic wind theory, winds typically follow isobars, but in the PBL, wind movement is altered by friction with the earth's surface and tends to cross isobars at angles of up to 30 degrees and proceed in the direction of the area of low pressure. The

friction effects on wind as stated above are relevant for all latitudes, despite the fact that the geostrophic wind theory is mostly indicative of winds in mid-latitudes.

Low-level jets are mainly nocturnal phenomena that are relatively strong horizontal winds in the lower section of the troposphere (Zhang et al., 2006). The first detected low-level jet was in Africa in the late 1930s (Farquharson, 1939), and it was later documented in other literature across other regions of the world (Blackadar, 1957; Bonner, 1968; Enfield, 1981; Parish et al., 1988; Zemba and Friehe, 1987). Rife et al. (2010) identified them in Ethiopia, Namibia, Angola, and the Tarim region in northwest China in their study on the global distribution of nocturnal low-level jets. In several literature, the distribution and characteristics of low-level jets have been thoroughly studied (Banta et al., 2002; Ranjha et al., 2013; Rife et al., 2010b; Wu et al., 2020a).

Low-level jets typically form near a sizable mountain range or areas where there are temperature differences between the sea and land (Stensrud, 1996). Numerous theoretical studies (Blackadar, 1957, 1957; Holton, 1967; Wiel et al., 2010), observations (Chen et al., 1994; Frisch et al., 1992; Lothon et al., 2008; Parish et al., 1988), and numerical simulations (Jiang et al., 2007; Kato, 1998; Parish and Oolman, 2010; Werth et al., 2011; Zhong et al., 1996) have been conducted to examine the characteristics of low-level jets and their effects on meteorology. Low-level jets are formed at a variety of meteorological scales, including synoptic (extratropical cyclones), mesoscale (weather fronts), and microscale (day-night surface heating). Low-level jets form in different ways depending on their location. Analyzing the vertical profile of the horizontal wind for the wind speed maxima is a major key in defining low-level jets. Additionally, low-level jets can be classified according to their location, timing, formation mechanism, and vertical structure (Ranjha et al., 2013). Nocturnal

low-level jet is the usual name for low-level jet that is detected at night (Blackadar, 1957). Also, coastal low-level jet is the name given to low-level jets that is observed offshore (Douglas, 1995; Doyle and Warner, 1991; Zemba and Friehe, 1987). Literature (Arritt et al., 1997a; Bentley and Mote, 1998; Cook et al., 2008; Helfand and Schubert, 1995; Jiang et al., 2007a; Mccorcle, 1988; Parish and Oolman, 2010a) also refers to low-level jets seen in the US Great Plains in recent studies as Great Plains low-level jets. Other studies that detected low-level jets in South America referred them as South America low-level jets (Marengo et al., 2004; Vera et al., 2006). Regarding their formation mechanism, low-level jets are typically divided into boundary layer jets (BLJs) and synoptic-system-related low-level jets (SLLJs). Low-level jets related to synoptic systems can be found in the atmospheric layer between 900 hPa and 600 hPa, and they are typically linked to synoptic-scale weather systems (Pham et al., 2008; Rife et al., 2010a). Boundary layer jets, in contrast to SLLJs, are low-level jets that develop in the PBL. The study's analysis of low-level jets is restricted to those that originate from the PBL. However, the two main processes by which low-level jets develops in the PBL are inertial oscillation and terrain-related baroclinicity (Blackadar, 1957; Holton, 1967). The PBL is decoupled from the surface by both processes. According to Holton (1967), the diurnal heating and cooling cycle of sloping terrain, which causes periodic variation in thermal wind and a subsequent low-level geostrophic wind, is what causes these jets to develop. According to Blackadar (1957), the production of low-level jets is a reaction to inertial oscillation caused by daytime surface heating during the night. Blackadar's idea cannot, however, account for other jet structures, such as the low-level jets across the Great Plains. Even though both hypotheses had their flaws, it is believed that they work best together to explain how low-level jets in the PBL form. Wexler (1961) suggested that topography is a key factor in the production of low-level jets in the Great Plains. He outlined

how the blockage of the easterly trade winds by rocky mountains is related to the genesis of the low-level jets over the Great Plains.

Additionally, low-level jets are thought to be a significant global mechanism for transporting moisture in the subtropical regions (Algarra et al., 2019). Due to its impact on weather, aviation safety, and regional climate, research on local precipitation in locations where low-level jets occur has increased (Gimeno et al., 2016). It is anticipated that the low-level jet dynamics may alter regional hydrological cycles. Low-level jets are closely connected with deep convection and nighttime precipitation, making them an essential component of the formation of mesoscale convective complexes (Bosart and Sanders, 1981; Maddox, 1983; Means, 1954a; Wallace, 1975;Zhang and Fritsch, 1986). Previous studies have documented linkages between low-level jets and rainfall extremes.

According to Higgins et al. (1997), the presence of low-level jets would cause a 48% increase in the low-level moisture flux from the Gulf of Mexico at night. In accordance with Arritt et al. (1997), a prolonged period of strong low-level jet activity was linked to the flood event that occurred in the US Great Plains in 1993. Besides, a low-level jet's exit zone is frontogenetic, lifting there destabilizes the PBL by moving an air parcel up to the level of free convection (Rife et al., 2010a). Precipitation happens near the jet's exit zone when a moist jet encounters a higher terrain. Low-level jets are also linked to the transportation of pollutants such as ozone from the residual layer to the stable boundary layer due to vertical diffusion (Udina et al., 2020). Low-level jets were linked to a well-mixed pollution daytime ozone reservoir in Baltimore-Washington DC on June 11th and 12th, 2015, with concentrations between 70 and 100 ppbv that decayed into a polluted nocturnal residual layer (Sullivan et al., 2017). Low-level jets in the Chinese city of Tianjin brought toxic air masses

from polluted industrial districts to the surface, increasing surface concentration (Ju et al., 2020) . In Tianjin, a city in China, low-level jets carried polluted air masses from polluted industrial regions to the surface which resulted in enhanced surface $PM_{2.5}$ concentration (Ju et al., 2020). Nevertheless, research indicates a threshold relationship between the onset of fog and northerly low-level jets (Wu et al., 2020). Inversion layer collapse and fog dissipation are caused by strong low-level jets, but weak low-level jets are more conducive to fog production because they reduce the intensity of the inversion and atmospheric stability (Wu et al., 2020).

1.2 Formation Mechanisms of Low-Level Jets

Many physical mechanisms have been described in the literature that explain how low-level jets form and develop all over the world. In order to evaluate physical parameterization schemes and model grid spacing for a certain numerical model to simulate low-level jets, it is vital to understand these mechanisms. The main physical mechanisms for the formation and development of low-level jets are listed here.

1.2.1 Inertial Oscillation

The theoretical analysis of low-level jets was emphasized by Blackadar (1957). According to his theory, eddy viscosity, which varies throughout the day, is what causes low-level jet formation. During the day, the air above the surface coupled with the surface in the midst of turbulence gives rise to internal friction in the PBL. The internal friction decreases the speed of winds making them subgeostrophic. The effect of turbulent mixing ceases when night falls, and frictional effects become less. As a result, the surface layer and the wind above the shallow nocturnal inversion decouples and are no longer in equilibrium. This results in an

imbalance between the coriolis and pressure gradient forces, which causes inertial oscillation of the wind. The period of this oscillation is around 17 hours in mid-latitudes, or half a pendulum day (Knippertz, 2008). Thus, wind speed maxima are created at approximately 8 hours after turbulent mixing has stopped (Hoxit, 1975).

1.2.2 Shallow baroclinicity

There are quite a number of mechanisms that generate baroclinicity over a region in the PBL. Strong low-level baroclinicity is produced in coastal regions or marginal ice zones where there has been a significant change in surface features due to horizontal differences in latent and sensible heat flow. Low-level baroclinicity causes intense geostrophic force with an orientation parallel to the low-level horizontal pressure gradient, which results in the formation of low-level jets. Low-level jets can generally have the same strength throughout the day if the horizontal temperature gradient found at sea-ice margins is constant.

However, low-level jets that do occur in coastal areas where surface fluxes include a diurnal component typically show a considerable changes in strength during the day. Furthermore, the effects of low-level baroclinicity brought on by sloping terrain can also result in the production of low-level jets. A horizontal temperature gradient will be generated by midday as a result of the impacts of diurnal heating on a sloping terrain where surface temperature is the same due to constant heat rate. The air above the higher terrain therefore warms up more than the air above the lower terrain as a result. When this happens, the air above the higher terrain is typically colder at night than air above lower terrain due to radiative cooling. Through this process, the horizontal temperature gradient develops a diurnal cycle, which causes the geostrophic wind to do the same. The geostrophic wind creates a jet-like vertical

wind profile by decreasing with height over higher terrain during the day and increasing with height at night.

Nonetheless, in coastal regions where surface fluxes have diurnal component, low-level jets that do occur usually have a significant diurnal changes in its strength. Furthermore, low-level baroclinicity is a characteristic of extratropical cyclones that often results in low-level jet streams over wide areas. Extratropical cyclones that formed on the Lee side of the Rocky Mountains are linked to low-level jet streams, according to Djurić and Damiani (1980). Additionally, as extratropical cyclones intensify, wind speeds in low-level jet streams may rise (Mahrt, 1981). The blockage of cold low-level air mass by a mountain range is another process that causes the development of low-level jet (Forbes et al., 1987; Parish, 2000). When a low-level flow cold, stable air mass meets a mountain range, there is a possibility of the cold stable air mass being trapped against the mountains. This produces a mesoscale horizontal temperature gradient normal to the mountains. If this process continues for long and the flow becomes geostrophically balanced, there is a likelihood for low-level jet to develop parallel to the mountain.

1.2.3 Terrain effects

In regions with complex terrain, diurnal heating produces both slope and valley winds that can cause low-level jets. In the mouth of Austria's Inn Valley, a down-valley wind system triggered the development of a low-level jet that attained a maximum speed of 14m/s at 200 m above ground level before sunrise (Pamperin and Stilke, 1985). Paegle and Rasch (1973) documented that terrain blocking due to intense stratification at night can produce a low-level jet. However, Great Plains low-level jets were found to be associated with boundary currents as a result of complex features of the terrain (Wexler, 1961). Low areas in terrain can

produce gap winds which other literature have observed to cause low-level jets. Gap winds do occur when large scale prevailing wind is accelerated through a channel between mountains owing to low-level horizontal pressure gradient. Walter and Overland (1984) detected low-level jets produced by gap winds over a domain of area $35\,km \times 200\,km$ in the United States.

1.2.4 Vertical parcel displacement

Low-level jets have been found to develop in response to vertical parcel displacement in some studies. In a model simulation of a secondary coastal cyclone, Uccellini and Kocin (1987) made several observations about low-level jet development with vertical parcel displacement. A change in vertical pressure gradient force occurs as a parcel approaches a developing cyclone in a baroclinic environment linked with a coastal front. A low-level jet formation is brought on by a rapid acceleration of a vertically displaced parcel caused by an increase in the ageostrophic wind component as the change increases (Uccellini and Kocin, 1987).

The explanation above shows that a variety of mechanisms can be used to explain how low-level jets develop, but none of them can fully account for the observations of low-level jets (Buajitti and Blackadar, 1957). They demonstrated how eddy viscosity variations throughout the day cannot adequately account for diurnal wind structure. But it was discovered that the combination of low-level baroclincity over sloping terrain and diurnally variable eddy viscosity is what causes wind variations linked to low-level jets (Bonner and Paegle, 1970). Additionally, Doyle and Warner (1991) noted that low-level jets over the Carolina are produced by both inertial oscillation and baroclinicity.

1.3 Simulation of Low Level Jets with WRF model

Numerical weather prediction models (NWP) are used as operational weather forecast models and are typically compressible, non-hydrostatic which are able to simulate a broad scale of meteorological phenomena driven by atmospheric stability such as low-level jets (Tay et al., 2021) compared to in-situ observations, NWP models offer a larger spatial and temporal coverage of wind climate studies. Understanding the geographic region of interest and parameterization schemes is necessary for using NWP models, which are noted for their improved accuracy in wind prediction and modeling outcomes (Dzebre et al., 2019). Before the advent of the Weather Forecasting and Research Model, accurately predicting the development, features, and position of low-level jets using numerical weather prediction (NWP) models was a significant difficulty. A numerical weather prediction system called the Weather Research and Forecasting Model (WRF) was created to meet the objectives of both operational forecasting and atmospheric research. The development of WRF model was a collaborative effort after much understanding on modeling of nocturnal stable boundary layers by researchers. WRF model uses nested domain runs that can be one-way or two-way coupled and enables for idealized or real-data simulation studies (Tay et al., 2021). The capability of the WRF model to simulate low-level jet events and near-surface wind-climate has been tested (Storm et al., 2009). The vertical and horizontal resolutions of the model grids, as well as the microphysics option, have a significant impact on the simulated flow inside the PBL (Aird et al., 2021). Research presented herein uses output from a simulation conducted using WRF model to characterize low-level jet occurrences over southern West-Africa.

1.4 Statement of the Problem

The low-level jet (LLJ) is closely related to severe rainfall events, air pollution, wind energy utilization, aviation safety, sandstorms, forest fire, and other weather and climate phenomena. Over the past five or six decades, researchers have conducted several studies on low-level jets and made substantial advancements. However, research on low-level jets over the southern part of West Africa has been taken into account but focused on the formation and breakdown of low-level jets and failed to address the frequency of its occurrences. To address the gap in literature, this study will analyze the frequency of occurrences of low-level jets in three bioclimatic regions found in the southern West Africa.

1.5 Goal and Objectives

The main goal of the study is to characterize low-level jets simulated with the WRF model in the planetary boundary layer (PBL) over southern West Africa. Specifically, the study aims;

i. To quantify the frequency of occurrence of low-level jets.

ii. To determine the direction of propagation of low-level jets.

iii. To determine the height of occurrence of the low-level jets.

1.6 Research Questions

i. How frequent do low-level jets occur over the three bioclimatic regions in southern West Africa?

ii. At what height in the palnetary boundary layer do these low-level jets occur?

iii. What is the direction of propagation of these low-level jets over each bioclimatic region in southern West Africa?

1.7 Significance of the Study

The study will first and foremost determine the frequency of low-level jets in each of the three bioclimatic regions found in southern West Africa. The region with the greatest number of occurrences will be named, and the cause of this will be discussed. Additionally, the months of the year with the highest frequency of low-level jet activity will be highlighted. However, the study will demonstrate that low-level jet is a nocturnal phenomenon by taking into account the times at which they are observed over southern West Africa. Moreover, the height at which these jets occur will be analysed. Nevertheless, the direction of propagation and the intensity of low-level jets within the three bioclimatic zones will be determined. All the findings in this paper will add more knowledge to quality weather forecast events in southern West Africa by meteorologists over the world.

1.8 Scope of the Study

Low-level jets identified in this research were simulated by the WRF model version 4.1.1. The model domian was limited to latitudes 3.9°N and 12.9°N and longitudes 16.0°W and 9.2°N which covers most parts of southern West Africa. A detection criteria similar to previous studies was used to detect low-level jets. Considered low-level jet characteristics in the analysis include frequency, intensity, time of occurence,height of occurence, and propagation direction.

1.9 Limitation of the Study

The researcher could not access 10 years (2012 – 2021) observation data from meteorological stations within the study region to evaluate the performance of the model simulation due to short timespan and archiving issues on the part of the meteorological stations. To address this issue, the researcher used ERA5 reanalysis data from ECMWF to evaluate the performance of the model by comparing it to WRF simulation data using statistical techniques.

1.10 Organization of the Dissertation

The dissertation is grouped into five chapters. The first chapter provides information of the background study, which involves introduction, literature review, problem statement, objectives, significance of the study and scope of the study. Chapter two is the theoretical background related to low-level jets formation. In chapter three, the study area andmethodology are discussed. Chapter four entails the results and discussions from this study. Chapter five contains conclusions and recommendations made by the study.

CHAPTER TWO

LITERATURE REVIEW AND THEORETICAL FOUNDATION

2.1 Literature Review

The description of the low-level jet and its variations in relation to synoptic scale forcing and large diurnal cycles has been the subject of several debates in the early stages. Low-level jets, according to Reiter, (1963) and Reiter and Whitney (1969), are those that have considerable vertical and horizontal shears as well as small-scale processes that produce jet-like vertical profiles and in which coriolis force plays a significant role.

Low-level jets, according to Bonner (1968), are three overlapping gaps that vary in size depending on the magnitude of the maximum wind speed. To produce a jet-like profile, the wind speed must drop below the height of the maximum by a threshold amount. Reiter (1963) and Reiter and Whitney (1969) did not agree with Bonner's concept of low-level jetsand other studies (Stensrud, 1996; Zhang et al., 2006) because the definition of a low-level jet is purely based on estimating the maximum low-level wind speed by analyzing the horizontal wind speed vertical profile. According to Bonner's climatology study from 1968, low-level jet occurs at night and reaches its greatest wind speed at about 800 meters above sea level. However, low-level jets are more common in the summer than the winter(Bonner, 1968). It is worth noting that, a significant west-to-east pressure gradient, such as the one found over the Great Plains, is a necessary favorable synoptic condition for the production of low-level jets (Bonner, 1968). Additionally, Mitchell et al. (1995) carried out a thorough climatological study over a 2-year period utilizing data from the wind profiler network. It was clear that low-level jets occur more frequently in late spring and early summer, when

southerly flow is more prominent and they traverse the southern and central Great Plains for 10 to 100 kilometers. At a site in the southern Great Plains, Whiteman et al. (1997) investigated the climatology of low-level jet using enhanced radiosonde observations. The findings showed that, around 2 am local time, 50% of low-level jet maxima occurred below 500 m.

Moreover, Blackadar (1957) relies on the retardation of subgeostrophic speeds of lower tropospheric air due to vertical, turbulent mixing with the heated surface throughout the day to explain the cycle of low-level jet as an inertial oscillation as provided in the background. He added that the height of the top of the nocturnal inversion matches with the height of the wind maximum, which is supergeostrophic at night. Hoecker (1963), on the other hand, focused on wind maxima as being supergeostrophic at night and occurring at a height between 300 and 700 m above ground level, albeit it does not always coincide with the height of the nocturnal inversion.

Hoecker (1963) added that various wind maxima can occasionally occur at various heights at the same time and place. However, (Hoxit, 1975) produced average profiles of diurnal fluctuations at the southeastern United States using rawinsonde data over nine years. The study found that mean wind speed maxima occurred near 500 m above ground level at 030 UTC, with the summer months showing the greatest diurnal variation in wind speed.

Additionally, in central Oklahoma in the United States, Crawford and Hudson (1970) examined wind data from six distinct observation levels. A 447 m high tower was used in the study, and the findings show that winds above the 90 m observation height are highest at night and lowest during the day, while winds below the 90 m observation height are lowest at night and highest during the day.

The study also found a clear diurnal pattern in the direction of the winds, which back during the day and veer at night. However, Wexler (1961) used Tepper (1954) and Veronis (1956) unbalanced current models to apply Charney (1955) inertial boundary theories to northward-flowing atmospheric jet streams found in the lowest 2 km over Central America. The trade wind was diverted to the north by the Central American continent's mountainous spine, which acted as a barrier to its westward motion. However, the unbalanced current's dynamic effect is the creation of pressure jumps and severe storms (Tepper, 1954; Veronis, 1956). This hypothesis was derived from a thorough mesoscale analysis by Tepper (1954) who suggested that pressure jumps with lengths of a few hundred kilometers and average duration of three to four hours occur in Northern Texas and Southwestern Oklahoma and move perpendicularly to the basic current and to the right with average wind speeds of about 20 m/s. These pressure jumps are three times more frequent at night than during the day.

Tepper (1954) exclusively looked at the baroclinic (or internal oscillation) mode of currents. Two issues with Tepper's (1954) analysis of the unbalanced southerly jet were raised by Veronis (1956): (i) the assumption that an initial unbalanced current can be as large as 20 m/s; and (ii) the exclusion of potential non-linear interactions between the baroclinic (internal oscillation) mode and the barotropic (free surface) mode. Wexler (1961) examined both works and found that there were few differences between the conclusions, supporting Tepper's (1954) assertion. As ground friction decreases during the night and has remained an issue to be resolved, no study was able to determine whether some pressure jump lines acquire their energy from the accelerating low-level jet. Porter et al. (1955) discovered that 75% of the squall lines that formed in the Great Plains had low-level jets.

Besides, over the Western Weddel Sea, Andreas et al. (2000) studied low-level jets and inversions. At the Ice Station Weddel (ISW), where there was sea ice covering the ground but no surface slope, the air boundary layer was profiled using radiosondes. With 96% of the soundings at the inversion layer at the surface and 44% of the inversions being surface-based, the results showed that the atmospheric boundary layer was mostly steady. In 80% of the soundings, the wind profiles clearly showed the presence of low-level jets. The jet core was consistently lower than 425 m in the 103 available soundings, with two thirds (2/3) of the jets occurring between 25 m and 175 m. The core of the jets' speed ranged from 3.0 m/s to 13.6 m/s, with the majority being between 4 m/s and 10 m/s (Andreas et al., 2000). Their research revealed that the jets were typically embedded in the inversion layer, which is frequently thought of as the atmospheric boundary layer's typical height. Ice Station Weddell (ISW) jets blew in all directions depending on their operation, with north and northeast as well as south and southwest orientations being the most prevalent. The jets' preferred orientation was southeast because of the baroclinicity that resulted from the surface temperature disparity between the ice-covered Weddel Sea and the open ocean to the north and east.

Additionally, Andreas et al. (2000) deduced the dynamics of the jets using the radiosonde profile's wind turning angles. Most of the angles were discovered to be positive, indicating that the Ekman dynamics-controlled jet rotates counterclockwise.

Low-level jet research has gained more attention as a result of evidence linking it to deep convective activity. First and foremost, according to Means (1954), low-level jets are mostly responsible for transporting moisture into areas of intense convection, which results in a region of rainfall that covers the whole state of Kansas.

Uccellini and Johnson (1979) pointed out that moisture and sensible heat transmission are connected to the development of low-level jets. However, Higgins et al. (1997) discovered that the presence of a low-level jet increases the low-level flow of moisture from the Gulf of Mexico at night by 48% over mean values. Furthermore, Arritt et al. (1997) demonstrated a connection between the extensive Great Plains floods and a prolonged period of intense low-level jets. However, low-level jets can enhance convection by combining divergence aloft from an upper-level jet (Beebe and Bates, 1955) with uplifting along the jet's nose (Zhong et al., 1996).

Low-level jets contribute to create a favorable thermodynamic environment for deep convection and may also be a mechanism for extending the lifespan of zones of convective activity, according to Beebe and Bates (1955). However, they do not by themselves promote the development of convective activity.

Furthermore, research on mesoscale convective complexes has brought attention to the connection between low-level jets and convective activity (Maddox, 1983). According to Maddox (1983), a strong low-level jet frequently occurs in both the precursor environment, where mesoscale convective complexes occur, and the environment of mature systems. Prior to the development of mesoscale convective complexes, the environment exhibits strong low-level convergence, warm advection, and ascending motion inside the low-level jet area. Furthermore, thunderstorms that begin in the late afternoon are typically where mesoscale convective complexes develop.

The development and evolution of low-level jets have been studied using a variety of numerical models. The case study method or model parameters are used in these studies to look at how sensitive low-level jets are to the initial boundary conditions.

First and foremost, a 2-dimensional numerical model by (McNider and Pielke (1981) demonstrated that terrain-induced pressure gradient force is a crucial component in the generation of low-level jets. Also, Paegle and McLawhorn (1973) revealed that using a soil hydrologic model to simulate jets, variations in soil moisture over sloping terrain have a significant impact on the structure and intensity of the jets. The development of low-level jets and their intensification as a result of latent heat of condensation are established by boundary layer processes, according to Nicolini et al. (1993), who observed this in their findings.

Gevorgyan (2018) investigated nine PBL parameterization schemes for the WRF model, analyzing which ones were most accurate at simulating low-level jets over Yerevan. TEMF, Mellor-Yamada-Janjic (MYJ), and Quasi-normal Scale Elimination (QNSE) Scheme exhibited better proficiency in the simulation of near-surface winds and clearly defined low-level jets among the nine schemes. Additionally, the identified jet cores occurred at heights between 150 and 250m above sea level, with winds that ranged from 12 to 21m/s.

Nevertheless, over the course of six months, Aird et al. (2021) used the results of high-resolution simulations with the WRF model to describe low-level jets over Lowa. A nested domain was used to run the WRF simulation. Both the outer and inner domains (D1 and D2) span $12\,km \times 12\,km$ and $4\,km \times 4\,km$ grid cells respectively. The inner domain's time step was 24s, whereas the outside domain's time step was 72s. A detection technique that deploys that the wind speed above and below the jet core must be below 80% of the jet wind speed within a vertical window of approximately 20-530m above ground level was used for the analysis. The results indicated the presence of low-level jets in at least all the $4\,km \times 4\,km$ grid cells over lowa with 98% of the occurrences during nighttime.

Additionally, the sources and sinks of moisture connected to nocturnal low-level jets (NLLJ) were recorded by Algarra et al. (2019). Using the FLEXPART Lagrangian model and ERA-Interim data from 1980 to 2016, it was possible to identify the main moisture source and sink zones as well as the behavior of low-level jets. 33 NLLJs regions were discovered by the study, with 20 in the north and 13 in the south. Also, marine regions serve as the sources of moisture transported by low-level jet over tropical latitudes. The Mediterranean Sea is identified as a significant source of moisture for low-level jets over northern Africa (Algarra et al., 2019). Low-level jets are connected to the moonsoon regimes in Asia and Australia, which are essential structures for transporting moisture. The overpopulated areas of Asia and the eastern coast of Africa, which are marked by heavy precipitation and low-level jets, have been designated as sink regions (Algarra et al., 2019).

To acquire more about the 3-dimensional structures and evolution of low-level jets over the Mid-Atlantic states in the warm seasons of 2001 and 2002, Zhang et al. (2006) conducted a case study with three model sensitivity simulations. 90% of low-level jets, with wind speeds ranging from 8 m/s to 23 m/s, were found to occur between the hours of 000 UTC and 060 UTC, according to the study. The majority of the low-level jets that were seen were westerly or southerly. According to sensitivity simulations, reducing the surface heat fluxes has the biggest impact on the development of low-level jets.

Moreover, Du et al. (2014) used the WRF model with a horizontal resolution of 9 km to characterize the spatial distributions and diurnal fluctuations of low-level jets in China. Low-level jets have been observed to exhibit clear diurnal fluctuations at night or in the early morning hours, and these variations are mostly brought on by inertial oscillation at night and vertical mixing in the PBL during the day. Additionally, Fiedler et al. (2013) conducted a

climatology study on the relationship between dust emissions over North Africa and nocturnal low-level jets (NLLJs). Statistics were utilized to evaluate NLLJs in 32 years of ERA-Interim reanalysis from ECMWF using a detection technique. The study discovered that in specific regions like the Bodele Depression and south of the Hoggar-Tibesti Channel, 80% of NLLJs occur in low-level baroclinicity and orographic settings, causing 15% of mineral dust emissions and 60% of overall total dust amount.

In addition, Du et al. (2012) used wind profiler radar data from Shanghai from 2008 to 2009 to examine the features of low-level jets during warm seasons. Boundary layer jets (BLJs) and synoptic related low-level jet stream (SLLJs) are two types of low-level jets that occur between 500 and 800m and 2100 and 2200m above ground level, respectively. In contrast to SLLJs, it was more obvious that BLJs were formed by the diurnal cycle, and both of them had distinct behaviors in terms of their temporal change in frequency of occurrences, the direction in which they occur, and how they are related to rainfall. The land-ocean thermal differential caused BLJs, which were mostly southerly winds produced by inertial oscillation with a high background southerly geostrophic wind. Again, BLJs are more frequent on days with rain than on days without.

Furthermore, Munday et al. (2021) study on Africa's low-level jets and their significance for rainfall and water vapor transport also found a link between strengthened low-level jets and drought in the continent's south and east at inter-annual timescales, with high low-level divergence and water vapor export acting as a break in the chain. Moreover, water vapor transmission from the Indian Ocean to the interior of Africa is dominated by NLLJs that are topographically limited. Once more, models with coarse resolution have trouble modeling a

well-defined low-level jet, yet it is essential to simulate low-level jets using climate models with horizontal resolution less than 60 km.

Again, Tay et al. (2021) used the WRF model to characterize mesoscale variability in low-level jet simulations. Low-level jets can be identified by their formation time, height, and intensity of their jet cores. With the use of the proper diagnostic tools, the boundary conditions and PBL schemes chosen were assessed. The results showed that the simulation's driving data, the ERA-Interim reanalysis, and the Mellor-Yamada Nakanishi Niino (MYNN) PBL scheme produced the greatest diagnostic scores for predicting surface temperature and wind speed. Ranjha et al. (2013) used gloabal ERA-Interim reanalysis data from 1980 to 2011 to document the seasonal variations of coastal low-level jets. According to the study, coastal low-level jets mostly occur in the summer and have a maximum wind speed of 9 to 15 m/s at a height of 500 to 700 above ground level.

Nonetheless, Jiménez-Sánchez et al. (2019) used the WRF model's finer horizontal, vertical, and temporal resolution over a 5-month period to define low-level jets across the Orinoco River basin. The Global Forecast System (GFS) analysis gave the WRF model's initial and boundary conditions. Over Colombia and Venezuela, Jiménez-Sánchez et al. (2019) reported low-level jets as a single stream tube with winds more than 8 m/s and 4 different jet cores that varied in height over sloping terrain. Additionally, January was the month with the highest recorded wind speed (13 m/s) and biggest spatial extent $(2{,}100\,km \times 400\,km)$. Early in the day is when mean wind speeds are at their highest (13–17 m/s), whereas late in the day is when they are at their lowest (8.9–9 m/s).

Lastly, Zhang and Meng (2019) used 45 warm-sector heavy rainfall episodes over southern China in 2013 and 2014 to assess the effectiveness of convection-permitting WRF model

simulation and examine at the general characteristics of low-level jets. They found that low-level jets are regularly present at both 800 and 925 hPa and is associated with 64% of warm-sector heavy rainfall occurrences along the coast. Due to a significant underestimating of coastal rainfall, the WRF model also shown a poorer QPF skill of the low-level jet type.

2.2 Theoretical Background

As discussed in chapter one, low-level jets formation are mainly caused by inertial oscillation and terrain related low-level baroclinicity. In this section, the study discusses the dynamics of the nocturnal lowlevel wind maximum in the PBL and thermal wind theory associated with baroclinicity over sloping terrain.

2.2.1 Inertial Oscillation

To begin with, lets consider a pressure gradient force, gravity and friction acting on an air parcel. When the three forces act on an air parcel, Newton's 2nd law can be written in the form of equation (2-1).

$$\frac{D\boldsymbol{U}}{Dt} = -2\boldsymbol{\Omega}\times\boldsymbol{U} - \frac{1}{\rho}\nabla P + \boldsymbol{g} + \boldsymbol{F}_r \qquad (2\text{-}1)$$

In equation (2-1), **U** is the velocity field of the air, **Ω** is the angular velocity vector of earth, ρ is the density of the air, P is the air pressure, $\boldsymbol{F}_r$ is the friction, g is acceleration due to gravity and (D/Dt) is the material derivative.

For a low-level horizontal flow, vertical motion is neglected. In the evening, the effect of friction on the horizontal flow reduces significantly and the flow decouples from the surface

area causing a diminishing of frictional force and no longer acts on the flow. Equation (2-1) can be expressed in cartesian coordinates with 'u' representing a eastward direction and 'v' a northward direction. As justified by Taylor-Proudman theorem, equation (2-1) is expressed into horizontal momentum equations as shown in equation (2-2) and equation (2-3).

$$\frac{du}{dt} = -\frac{1}{\rho}\frac{\partial p}{\partial x} + fv \tag{2-2}$$

$$\frac{dv}{dt} = -\frac{1}{\rho}\frac{\partial p}{\partial y} - fu \tag{2-3}$$

where (du/dt) and (du/dt) are accelaration of the horizontal flow in eastward and northward direction respectfully. $(f = 2\Omega \sin\phi)$ is the coriolis vector which is needed to produce the oscillation of the low-level flow (Markowski and Richardson, 2011). The low-level flow can be partitoned into geostrophic (g) component and ageostrophic (a) component for each eastward and northward flow as illustrated in equation (2-4) and (2-5)

$$u = u_g + u_a \tag{2-4}$$

$$v = v_g + v_a \tag{2-5}$$

Now, equations (2-4) and (2-5) are substituted into equations (2-2) and (2-3). In doing so, $(dv_g/dt = 0)$ because it is assumed horizontal pressure gradient is constant in time. The expression for $(\boldsymbol{v_g} = (1/\rho f\boldsymbol{k}) \times \nabla_h p)$ and $(d\boldsymbol{v_g}/dt = \partial \boldsymbol{v_g}/\partial t + \boldsymbol{v}.\nabla \boldsymbol{v_g})$ according to Markowski and Richardson (2011). Since horizontal pressure gradient is assumed constant in time such that $(\partial \boldsymbol{v_g}/\partial t)$, the derivative of the horizontal pressure gradient will be zero

$(\nabla(\nabla_h p)=0)$ as presented by Markowski and Richardson (2011, p.107). The results are shown in equations (2-6) and (2-7).

$$\frac{du_a}{dt}=-\frac{1}{\rho}\frac{\partial p}{\partial x}+f(v_g+v_a) \tag{2-6}$$

$$\frac{dv_a}{dt}=-\frac{1}{\rho}\frac{\partial p}{\partial y}-f(u_g+u_a) \tag{2-7}$$

The eastward and northward directions of the geostrophic component of the horizontal flow is defined in equations (2-8) and (2-9).

$$u_g=-\frac{1}{\rho f}\frac{\partial p}{\partial y} \tag{2-8}$$

$$v_g=\frac{1}{\rho f}\frac{\partial p}{\partial x} \tag{2-9}$$

Now, equations (2-8) and (2-9) is substituted into the momentum equations (2-6) and (2-7) to obtain equations (2-10) and (2-11).

$$\frac{du_a}{dt}=-\frac{1}{\rho}\frac{\partial p}{\partial x}+f\frac{1}{\rho f}\frac{\partial p}{\partial x}+fv_a \tag{2-10}$$

$$\frac{dv_a}{dt} = \frac{1}{\rho}\frac{\partial p}{\partial y} - f\frac{1}{\rho f}\frac{\partial p}{\partial x} + fu_a \tag{2-11}$$

The pressure gradient terms in equations (2-10) and (2-11) cancels out with leads to equations (2-12) and (2-13).

$$\frac{du_a}{dt} = fv_a \tag{2-12}$$

$$\frac{dv_a}{dt} = -fu_a \tag{2-13}$$

Equations (2-12) and (2-13) have two unknowns. The study seek to find for the first unknown by first taking the derivative of equation (2-12) with respect to time and then substitute the results with equation (2-13) to obtain equation (2-14).

$$\frac{d^2u_a}{dt^2} = f\frac{dv_a}{dt} = -f^2u_a \tag{2-14}$$

Now, from equation (2-14), if f is treated as a constant, it becomes a second order linear differential equation with a characteristic equation $a^2+1=0$ with real roots of $(1\pm i)$ thereby having a general solution with constant cofficients as shown in equation (2-15)

$$u_a = D_1\cos ft + D_2\sin ft \tag{2-15}$$

To find for the second unknown, make the unknown the subject from equation (2-12) to obtain equation (2-16).

$$v_a = \frac{1}{f}\frac{du_a}{dt} \tag{2-16}$$

Now, substitute equation (2-15) into equation (2-16) to obtain (2-17) and solve the derivative to obtain (2-18)

$$v_a = \frac{1}{f}(-D_1 f \sin ft) + \frac{1}{f}(D_2 f \cos ft) \tag{2-17}$$

$$v_a = -D_1 \sin ft + D_2 \cos ft \tag{2-18}$$

At t = 0, define $u_a = u_o$. Therefore,

$$u_o = D_1 \cos 0 + D_2 \sin 0 \tag{2-19}$$

$$u_o = D_1 \tag{2-20}$$

Similarly, at t = 0, define $v_a = v_o$. Therefore,

$$v_o = D_1 \cos 0 + D_2 \sin 0 \tag{2-21}$$

$$v_o = D_2 \tag{2-22}$$

Finally, the equations for the ageostrophic flow are

$$u_a(t) = u_o \cos ft + v_o \sin ft \tag{2-23}$$

$$v_a(t) = v_o \cos ft - u_o \sin ft \tag{2-24}$$

Equations (2-23) and (2-24) can be rewritten as equations (2-25) and (2-26) using trigonometric identities.

$$u_a(t) = |v_o| \cos(\psi_o - ft) \tag{2-25}$$

$$v_a(t) = |v_o| \sin(\psi_o - ft) \tag{2-26}$$

In equations (2-24) and (2-25), $v_o = (u_o, v_o)$, $|v_o| = \sqrt{(u_o^2 + v_o^2)}$, and ψ_o is the angular constant which determines the orientation of the ageostrophic wind. Equations (2-25) and (2-26) show that the ageostrophic wind rotates clockwise in a circular pattern within the northern hemisphere once the adjustment process begins following the cessation of decoupling of the boundary layer and deep mixing (Markowski and Richardson, 2011). A full circular path is completed by the ageostrophic wind vectorat $t = 2\pi/f$ and a full revolution is achieved at $T = 12h/\sin\phi$ where ϕ is the latitude. The wind become supergeostrophic 10 hours after the start of the adjustment process such that $\phi = 30^o$.This usually occurs at 3am to 4am local time and the intensity of the supergeostrophic winds depends on how subgeostrophic the wind was in the late afternoon (Markowski and Richardson, 2011).This means that days where there is abundant insolation, deep mixing and deep boundary layers, winds are supergeostrophic at night yielding a low-level jet.

2.2.2 Baroclinicity Over Slopping Terrain

In this section, we consider the thermal wind theory and its relation to low-level baroclinicity over slopping terrain as proposed by Holton (1967).

To begin with, let's recall the thermal wind relation,

$$\frac{\partial u_g}{\partial z} = -\frac{g}{f T_m}\frac{\partial T_m}{\partial y} \tag{2-27}$$

$$\frac{\partial v_g}{\partial z} = -\frac{g}{f T_m}\frac{\partial T_m}{\partial x} \tag{2-28}$$

where T_m is the mean layer temperature.

During dayttime, the west-to-east temperature gradient is negative $(\partial T_m/\partial x<0)$near the ground and aloft over slopping terrain because solar insolation warms ground and forms a mixed layer with near adiabatic lapse rate (Markowski and Richardson, 2011). This implies that $(\partial v_g/\partial z<0)$.

However, during nighttime the ground of the slopping terrain cools more quickly than the air above it which results in west-to-east temperature gradient being positive $(\partial T_m/\partial x>0)$. Thus, $(\partial v_g/\partial z>0)$. This creates a temperature inversion. Above the temperature inversion level, the gradient may be negative $(\partial T_m/\partial x<0)$ as well as the thermal wind $(\partial v_g/\partial z<0)$ according to Markowski and Richardson (2011)

The above mechanism implies that the geotrophic wind vector reaches maximum near the nocturnal inversion level which means the actual wind vector would reach a larger maximum

than could be achieved strictly through the release of friction (Markowski and Richardson, 2011). The lack of deep mixing (stability) of the air below the nocturnal inversion helps the low-level jet to persist. Moreover, in the analysis of the nocturnal wind maxima in section 2.1, the assumption that $dv_g/dt=0$ is false as shown by the thermal wind theory over slopping terrain in the Great Plains (Markowski and Richardson, 2011). The thermal wind theory does not explain the mechanism of supergeostrophic wind. In situations were diurnal changes in $\vec{v}_g$ on inertial oscillation is imposed on $\vec{v}_a$, low-level jet magnitude is changed. In this case, inertial oscillation theory is best used together with thermal wind theory (Markowski and Richardson, 2011).

CHAPTER THREE

DATA AND METHODOLOGY

3.1 Study Area

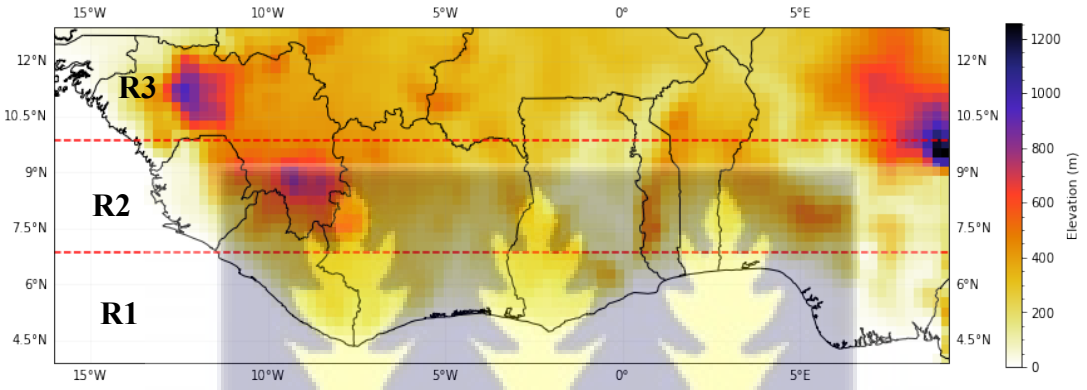

Figure 3.1: Weather Research Forecast (WRF) domain of the Study

According to Figure 3.1, the study region is in the southern section of West Africa, between latitudes 3.9°N and 12.9°N and longitudes 16.0°W and 9.2°N. The Gulf of Guinea borders it on the south and west, the Sahel on the north, and western Nigeria on the east. The Guinean Highlands and the Jos Plateau in central Nigeria typically have the highest terrain elevations within the research area, ranging from 1000 to 1260 m. The study area is characterized by mainly three different bioclimatic regions: the first is the West Sudanian Savanna Region (R3) which is located within latitude 9.9°N to 12.9°N. The climate is tropical savanna, hot, and semi-arid, with temperature ranges of 30 to 33 degrees Celsius in the summer season and 18 to 21 degrees Celsius in the winter. In the south and north of the savanna zone, respectively, annual precipitation ranges from 600 mm to 1000 mm, with ecologically dry seasons lasting 5–7 months (Cotlion & Tappan, 2016). The second zone is the Guinean Region (R2), which is located between latitudes 6.9°N and 9.9°N and is immediately south of the Sudanian Region. Within the zone, there are both inland mountains and forests as well

as coastal lowlands. With a distinct dry season lasting 7 to 8 months, the average annual rainfall ranges from 1,200 mm to 2,200 mm (Cotlion & Tappan, 2016). The Guineo-Congolian Region (R1), which is located immediately south of Guinean Region and borders the Gulf of Guinea, is the third region. It is situated between latitudes 3.9° and 6.9°N. This region is the wettest of them all, with annual rainfall ranging from 2,200 to 5,000 mm (Cotlion & Tappan, 2016). Geographically, the region is split into western and eastern blocks separated by Dahomey Gap. The average wind speed in Guineo-Congolian Region is 3-5 m/s.

3.2 WRF Configuration

In this work, a high resolution WRF model version 4.1.1 was used to run a 10-year simulation on low-level jets over a single domain that covers most of southern West Africa and spans 28 km × 28 km grid cells. The WRF simulations lasted ten years, from 000 UTC on January 1, 2012, to 180UTC on December 31, 2021. For DO1, a time step of 180 s and 55 vertical sigma levels were used. This suggests that simulations were run at 000 UTC, 030 UTC, 060 UTC, 090 UTC, 120 UTC, 150 UTC and 180 UTC. There are 21 levels below 1500 m above ground level that enables a fine vertical resolution to evaluate atmospheric processes within the PBL. The WRF model's upper atmosphere is situated at a pressure of 50 hPa. The simulation's forcing data were Global Forecast System datasets (GFS). The National Centers for Environmental Prediction (NCEP) uses the Global Forecast System (GFS) weather forecast model to produce data for a wide range of atmospheric and land-soil variables, such as temperatures, winds, precipitation, soil moisture, and air ozone concentration. The system combines four distinct models (atmosphere, ocean, land/soil, and sea ice) that cooperate to describe meteorological conditions accurately.

Using GFS analysis and forecast, the WRF model's boundary conditions were established. The boundary conditions were specified in the WRF runs at 3-hourly temporal resolution. The key physics settings in the WRF model are schemes widely used for high resolution simulations: the WRF Single Moment -6 class graupel microphysics scheme (Hong and Lim, 2006), Rapid Radiative Transfer Model (RRTM) longwave radiation scheme (Mlawer et al., 1997), Dudhia shortwave radiation scheme (Dudhia, 1989), Mellor-Yamada-Nakanishi-Niino (MYNN) 2.5 level TKE boundary layer scheme (Nakanishi and Niino, 2009) along with the Noah land surface model (Tewari et al., 2004) and Grell 3D Ensemble cumulus option scheme (Grell and Dévényi, 2002). Simulation of low-level jets in the Southern part of West Africa is highly sensitive to the choice of land surface model and PBL parametirization schemes because of its unique bioclimatic regions. The Noah land surface scheme was chosen because it accounts for vegetation effects, forecasts soil temperature and moisture in four layers, and offers heat and moisture fluxes for the PBL, the Noah land surface method was chosen. The MYNN scheme uses vertical mixing based on local turbulent kinetic energy in the PBL and free atmosphere, and it has already been approved for use in low-level jet simulation in the Great Plains. Studies have demonstrated that the MYNN scheme, particularly with high model top pressure levels (50 hPa) and precise vertical grid spacing, delivers the least mean absolute error when modeling critical jet core conditions (Samman and Gallus., 2018; Smith et al., 2018). Analysis presented in this study use model output sampled monthly for January 2012 to December 2021 and thus considers 2,250 vertical wind profiles for selected grid cells within the domain. Wind speeds below 1800 m were considered for easy identification of low-level jets in the PBL.

3.3 Sources of WRF model Uncertainties

Uncertainties in WRF models are caused by model structure, calibration (observation), and input data. In addition to these factors, model initial and boundary conditions may also contribute to uncertainty. Effective parameters are parameterizations that come from conceptual simplifications and are frequently found in WRF models. The inability to predict or measure these useful factors that integrate and conceptualize processes might lead to parameter uncertainty (Beven, 1989). On the other hand, even if a model accurately represents the hydrologic system, parameter uncertainty may still exist because of flaws in the calibration data. The difficulty of assessing natural variability, the presence of observation errors, and the inability to estimate effective parameters precisely all contribute to parameter uncertainty (Beven, 1989).

Nevertheless, model performance is strongly influenced by model structures (Rojas, 2008), so structural uncertainty is important as it can make the model and quantification of other uncertainties useless (Rojas, 2008). Comparing structural and parameter uncertainty, Højberg et al. (2005) findings showed that structural uncertainty is significantly greater than parameter uncertainty.

Moreover, different hydro-meteorological, catchment, and subsurface data provide input forcing for WRF models. The data utilized for model forcing are sparse and vulnerable to gaps, imprecisions, and uncertainties, despite advancements in data gathering and processing. The majority of the time, input data are scaled, interpolated, and derived from other measurements, resulting in an uncertainty range of 10–40% (McMillan, 2018). These data input errors are called input uncertainty. Inaccurate parameter estimate might result from failing to take input uncertainty into account.

3.4 Detection Criteria for Low-Level Jets

Several criteria for low-level jets identification has been developed by previous studies. This study employs a relative and absolute detection criteria similar to (Baas et al., 2009). It requires that

i. The wind speed maximum and the minimum above in a vertical wind profile must occur below 1800 m

ii. The wind speed maximum must be at least 2 m/s stronger than the minimum above (absolute criterion)

iii. The wind speed maximum must be at least 25% stronger than the minimum above (relative criterion)

The reason for applying absolute criterion is that in very calm wind conditions, it prevents small variations in wind speed with height accidentally being identified as low-level jets. Also, the reason for applying a relative criterion is that, in cases of high wind speed, it prevents the situation where the absolute criterion may be mistakenly satisfied (Baas et al., 2009). Considering the domain of the study, ground-level obstacles such as vegetation and topographic features tend to slow the wind near the surface. Because the effect of these ground-level obstacles decreases with height above ground, wind speeds tend to increase in height above the ground. Therefore, the height was set at 370 m above ground to obtain a well defined wind profile as shown in Figure 3.2. For a given vertical wind profile as shown in Figure 3.2, if both criteria of low-level jet identification are met, the maximum (red dot) is declared as a low-level jet. The violet dots in Figure 3.2 illustrates the local minimums above the maximum.

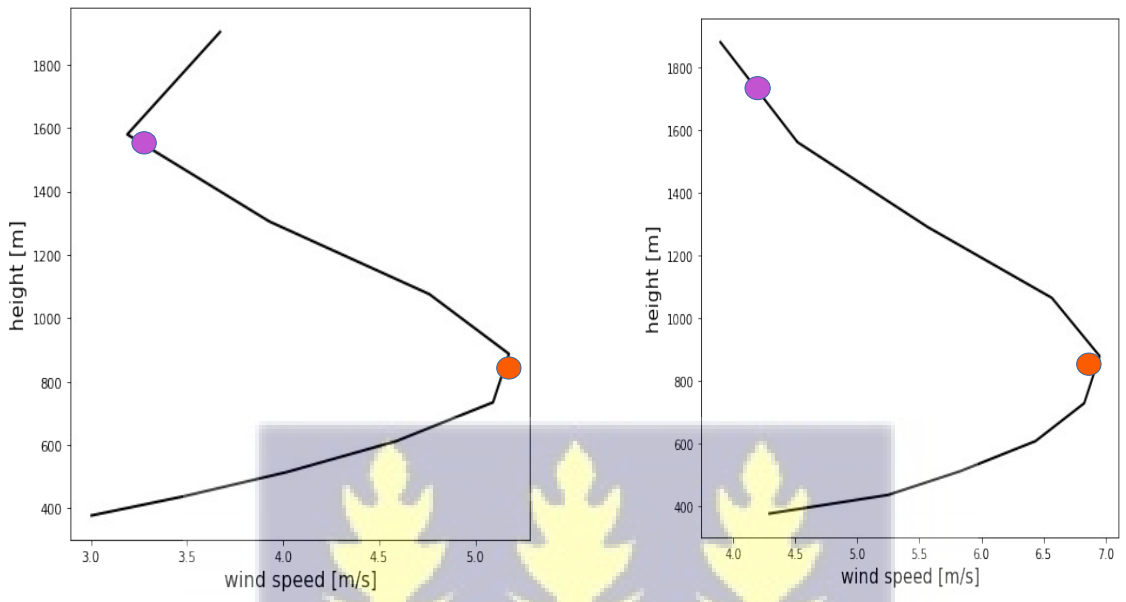

Figure 3.2: Schematic diagram showing the detection algorithm of low-level jets in this study. Red dots show local maximums, violet dots show local minimums. Source: Field data

3.5 Validation Techniques

Statistical techniques were used to validate the simulations from the WRF model. Simulation datasets are compared to observational datasets using the statistical tools listed below to check for its accuracy. The observational datasets used are ERA5 reanalysis data from the European Centre for Medium-Range Weather Forecasts (ECMWF). A significant number of atmospheric, land, and oceanic climate variables are provided hourly estimates by ERA5. The data span the planet on a grid of 30 km, and they use 137 levels to resolve the atmosphere from the ground up to an altitude of 80 km. Reduced geographical and temporal resolutions for all variables are included in ERA5's information regarding uncertainty. The horizontal resolution was set to 28 km similar to the WRF output. The atmospheric variable used for the validation is 10 m wind speed from both datasets. The coefficient of

determination, mean absolute percentage error (MAPE), the root mean squared error (RSME) and the mean absolute error (MAE) are used to evaluate the model performance.

3.5.1 Coefficient of Determination (R^2)

Based on the proportion of the overall variation in outcomes that the model is able to account for, the coefficient of determination quantifies how well observed events are predicted by the model. Its value is between 0 and 1. A simulation's results can be perfectly predicted if R squared is equal to 1, and the opposite is true if R squared is equal to 0. It is written as

$$R^2(y, \hat{y}) = 1 - \left[\frac{\sum_{i=1}^{n}(y_i - \hat{y}_i)^2}{\sum_{i=1}^{n}(y_i - \bar{y}_i)^2}\right] \quad (3\text{-}1)$$

where y is he observation data (ERA5) and ŷ is the simulated data (WRF) for the evaluated constituent respectively.

3.5.2 Mean Absolute Percentage Error

The accuracy of a forecast derived from a model is measured by the mean absolute percentage error (MAPE). MAPE is calculated using

$$\text{MAPE}(y, \hat{y}) = \frac{1}{n}\sum_{i=0}^{n-1}\frac{|y_i - \hat{y}_i|}{\max(\epsilon, |y_i|)} \quad (3\text{-}2)$$

where y is he observation data (ERA5) and ŷ is the simulated data (WRF) for the evaluated constituent respectively. Table 3.1 below indicates the interpretation of MAPE score.

Table 3.1: Interpretation of MAPE score (Source: Lewis(1982))

MAPE	Interpretation
< 10%	Highly accurate forecasting
10% - 20%	Good forecasting
20% - 50%	Reasonable forecasting
> 50%	Inaccurate forecasting

3.5.3 Root Mean Squared Error

The difference between the model's predicted values and the actual values is measured by the root-mean-square error (RMSE). An absolute fit to the data is indicated by a zero value for RMSE, which is always non-negative.

RMSE is computed as

$$\mathrm{RMSE}\left(y, \hat{y}\right) = \sqrt{\frac{1}{n}\sum_{i=0}^{n-1}\left(y_i - \hat{y}_i\right)^2} \qquad (3\text{-}3)$$

where y is he observation data (ERA5) and $\hat{y}$ is the simulated data (WRF) for the evaluated constituent respectively. It is worth noting that the smaller the RMSE score, the closer the predicted and observed values are.

3.5.4 Mean Absolute Error (MAE)

The mean of the absolute difference between model prediction and observation values is given by the mean absolute error. Calculating MAE involves

$$MAE(y,\hat{y}) = \frac{1}{n}\sum_{i=0}^{n-1}|y_i - \hat{y}_i| \qquad (3\text{-}4)$$

where y is he observation data (ERA5) and ŷ is the simulated data (WRF) for the evaluated constituent respectively. It is worth noting that the smaller the MAE score, the closer the predicted and observed values are.

CHAPTER FOUR

RESULTS AND DISCUSSIONS

4.1 Results of the Study

In this section, WRF simulation results, the frequency of occurrence of low-level jets, the height of occurrence of low-level jets and the direction of propagation of low-level jets are mentioned.

4.1.1 WRF Simulation Results

Using the statistical methods indicated in section 3.5, the performance of the WRF simulation over the study's domain is validated in this section. The regressional plots of simulated WRF versus ERA5 reanalysis data for each year over the whole study domain are shown in Figure 4.1. With coefficient of determination (R^2) ranging from 0.605 to 0.868, the simulated WRF is relatively close to that of ERA5. There is a positive correlation between the two datasets, as indicated by the linear regression equations' slope magnitudes, which range from 0.49 to 0.80 and are less than 1. However, the root mean squared error (RMSE), mean absolute percentage error (MAPE), and mean absolute error (MAE) statistical performance measures, as provided in Section 3.5, are used to evaluate the performance of the WRF model over the three bioclimatic regions. The statistical performance of the WRF model throughout the three bioclimatic areas are summarized in Figure 4.2. Figure 4.2 indicates that, the overall performance of the simulated WRF is better in the Guineo Congolian region (R1) compared to the other two regions with very minimal errors. This outcome is consistent with (Soares et al. 2014), finding that offshore regions had the lowest

errors when evaluating WRF simulated surface winds at Iberia. The RMSE score ranges from 0.13 to 0.25 (Figure 4.2(a)), MAPE scores ranges from 3.71% to 7.21% (Figure 4.2(b)) and MAE score ranges from 0.11 to 0.23 (Figure 4.2(c)) in the Guineo Congolian region (R1). The performance of the simulated WRF is relatively better in West Sudanian Savanna Region (R3) than the Guinean Region (R2). In the West Sudanian Savanna Region (R3), the RMSE score range is 0.22 to 0.59 (Figure 4.2(a)), MAPE score range is 7.21% to 23.49% (Figure 4.2(b)) and MAE score range is 0.18 to 0.59 (Figure 4.2(c)). Moreover, in the Guinean Region (R2), the RMSE score range is 0.21 to 0.65 (Figure 4.2(a)), MAPE score range is 8.91% to 29.12% (Figure 4.2(b)) and MAE score range is 0.21 to 0.64 (Figure 4.2(c)). The agreement between the ERA5 reanalysis and modelled surface wind speeds show that WRF simulation produces realistic regional results, giving the study confidence in the ability of the model to simulate low-level jets over southern West Africa.

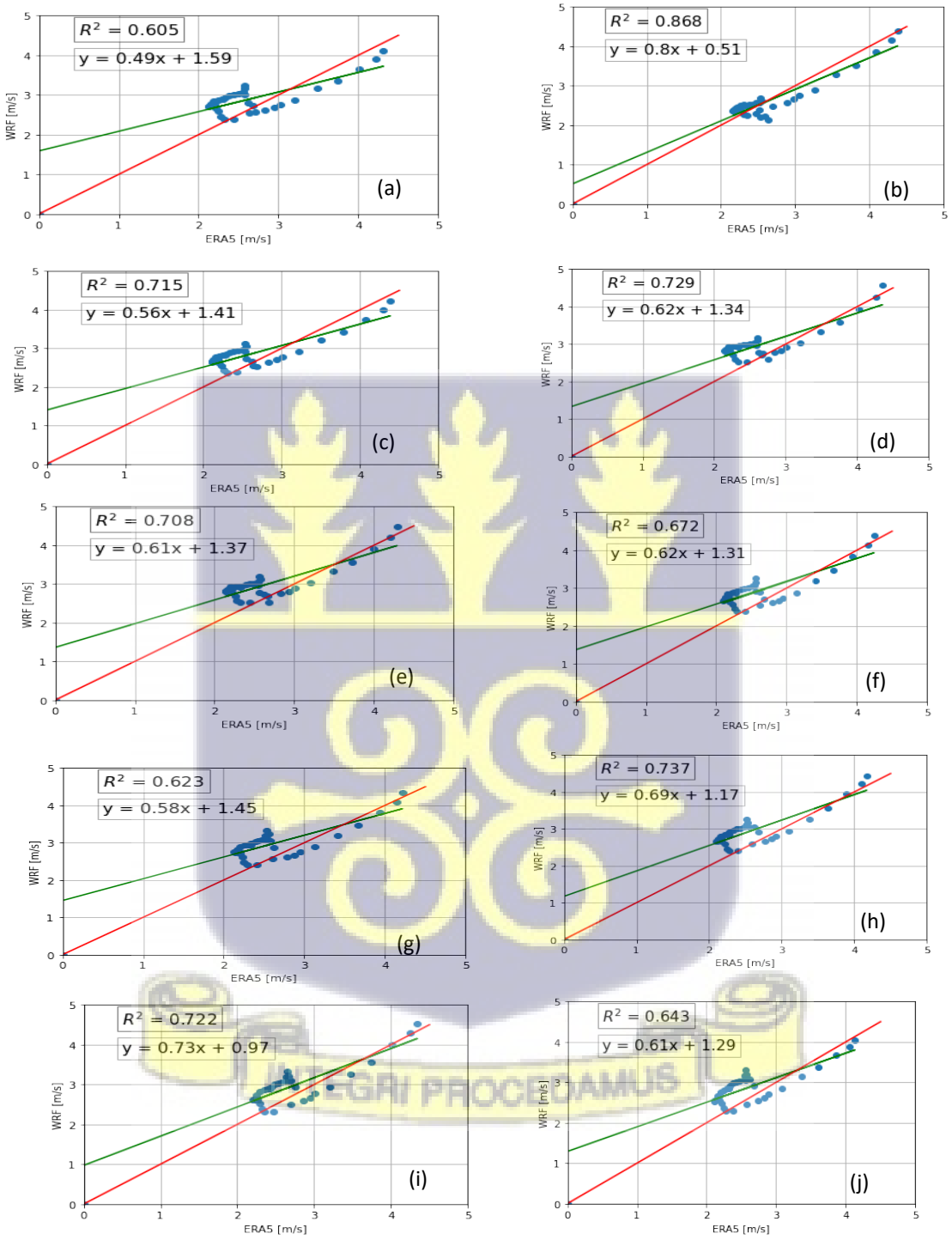

Figure 4.1: Regressional plots of stimulated WRF vs observed ERA5 reanalysis data (a) 2012 (b) 2013 (c) 2014 (d) 2015 (e) 2016 (f) 2017 (g) 2018 (h) 2019 (i) 2020 (j) 2021

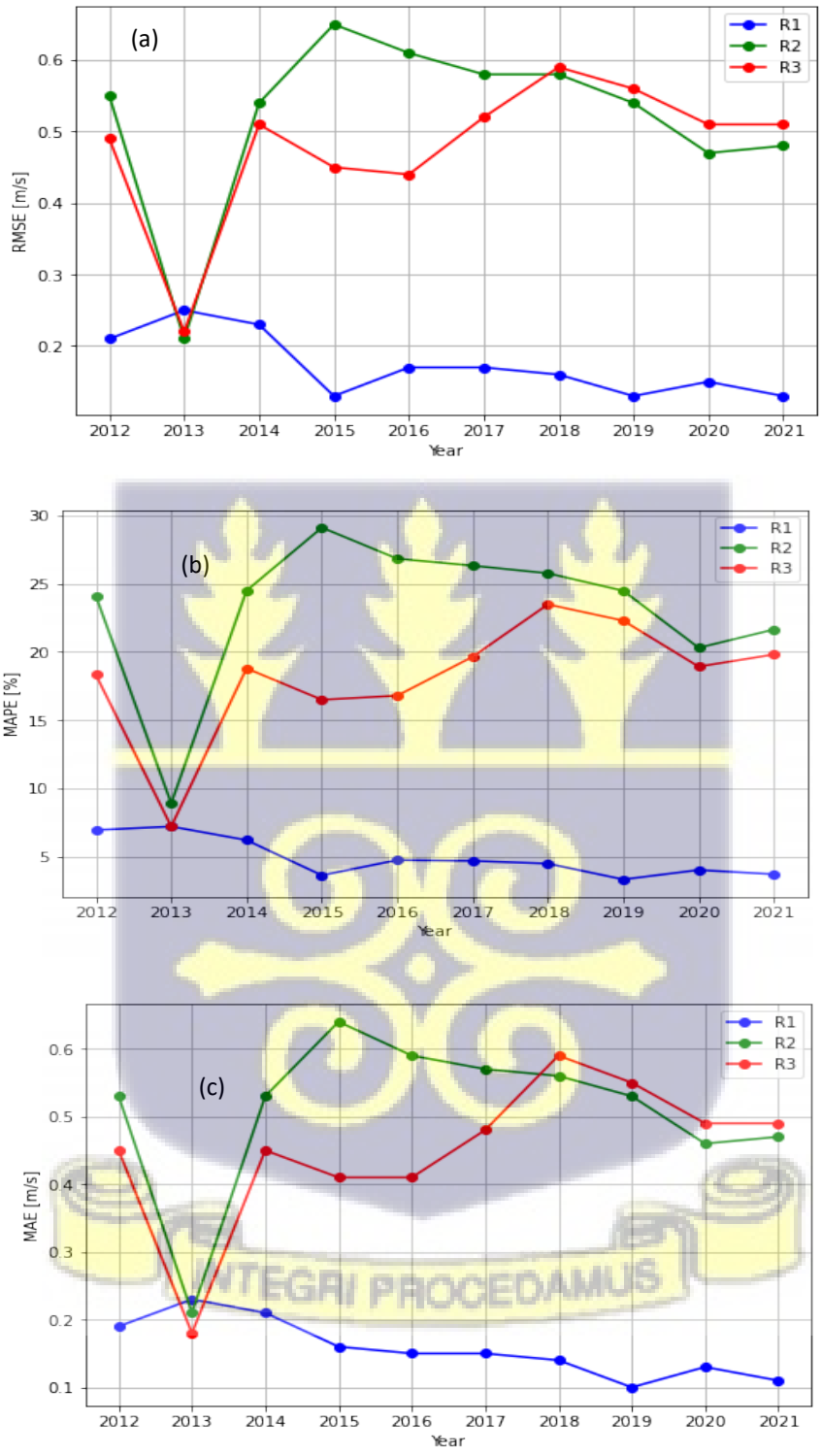

Figure 4.2: Line plots showing the statistical measures for simulation accuracy over (a) Root mean squared error (RMSE) (b) Mean absolute percentage error (MAPE) (c) Mean absolute error (MAE).

4.1.2 Frequency of Occurrence of Low-level jets

For the seven (7) different hours in a day indicated in section 3.2, a total of 2,520 monthly averaged vertical wind speed profiles are plotted over the study's region.. Applying the study's detection criteria of low-level jets on the vertical wind speed profiles, 1,043 (41.4%) low-level jets profiles and 1,477 (58.6%) non low-level jets profiles are observed (Figure 4.3(a)). Among the 41.4% low-level jet profiles detected, region R1, R2 and R3 have 406 (40%),324 (31.1%) and 324 (31.1%) recorded low-level jet profiles respectively (Figure 4.3(b)). The study's definition of a low-level jet profile is a vertical wind speed profile in which the wind maxima is declared as a low-level jet when the detection criteria are met. Figure 4.3(c) illustrates that low-level jet profiles are detected in each year of the period of study. The three regions in which the low-level jet profiles are found are compared for each year (Figure 4.3(c)). The comparison is based on how frequent each region records low-level jets each year and the variation between the highest and lowest occurrences. From Figure 4.3(c), the highest percentage variation between the maximum and minimum occurrence are 12.3%, 11.5%, 11.4%, 10.5% , and 10.1% in the years 2013, 2018, 2021, 2012 and 2016 respectively. Also, 40% of low-level jet profiles are observed in R1, 32.3% in R2 and 27.7% in R3 for the year 2013. The year 2018 has 38.57% of observed low-level jet profiles found in R1, 27.1% in R2 and 34.4% in R3. Also, the year 2021 has 40.7% of observed low- level jet profiles in R1, 30.1% in R2 and 29.2% in R3 (Figure 4.3(c)). However, 39.5% of detected low-level jet profiles are found in R1, 29.0% in R2 and 31.5% in R3 in 2012 (Figure 4.3(c)). In 2016, 37.6% low-level jet profiles detected are found in R1, 27.5% in R2 and 34.9% in R3 (Figure 4.3(c)). Nonetheless, the percentage of detected low-level jet profiles found in the years 2014, 2015, 2017, 2019 and 2020 in the three regions did not show much difference

(Figure 4.3(c)). The lowest average percentage difference between the highest and lowest occurrence in the three regions is 5% . Generally, the frequency of low-level jet profiles found for each year have the greatest percentage in R1. Also, the frequency of detected low-level jets profiles in R3 are relatively higher than the detected low-level jet profiles in R2 for 6 years (2012, 2016, 2017, 2018, 2019 and 2020) out of the 10 years of study as shown in Figure 4.3(c).

Besides, Figure 4.3(d) illustrates how frequent low-level jet profiles are detected in the months of the year. In this case, the number of detected low-level jet profiles from the 3 regions are grouped in each month of the year. Likewise for the yearly groupings, the 3 regions are compared on the basis of the region with the highest detected low-level jet profiles in a particular month. This enables stakeholders to know the particular months that low-level jets frequently occur over the study's domain since they are known by several literatures to play in significant role in our weather. In Figure 5d, the maximum frequency (13.8%) of detected low-level jet profiles are found in the month of August in R1. The month of July is second to August for the most frequency (13.3%) of detected low-level jet profiles in R1. The months with the minimum occurrences in R1 are December and January with frequencies of 5% and 5.2% respectively. In region R2, August (11.1%) and February (11.1%) are the months with the maximum frequency of detected low-level jets profiles. The minimum frequency of detected low-level jets in R2 occurs in November (5.5%) and December (5%). Futhermore, region R3 found its maximum frequency of detected low-level jets profiles in February (10.9%) and January (9.6%). The minimums are found in the months of September (5.1%), October (5.4%) and November (4.8%). However, the study observed all 3 regions have a rise in frequency of detected low-level jet profiles from January to February as shown in Figure 4.3(e). There is a decrease from February to May in the

frequency of detected low- level jet profiles and takes a rise to the month of August (Figure 4.3(e)). Besides, the frequency declines to the minimum in December for R1 to R2 and November for R3 (Figure 4.3(e)). The frequency of detected low-level jet profiles in R1 and R2 takes a rise in January but R3 takes it rise in December (Figure 4.3(e)). On the average, the highest frequencies of detected low-level jet profiles are found in February, July and August (Figure 4.3(e)). The study also demonstrated the time of occurrences of these low-level-jets for seven (7) different hours in each day. In the simulation, the study employed a model time-step of 180 s as mentioned in Section 3.2. This means that the model simulated low-level jets in 3 hour interval starting from 000 UTC to 180 UTC. The frequency of occurrence of detected low-level jet profiles are grouped per the hours they occur as shown in Figure 4.3(f). From Figure 4.3(f), it is evident that majority (32.9%) occur at 000 UTC and the second (26.6%) occur at 030 UTC. At 060 UTC and 090 UTC, 21.4% and 13.6% of low-level jet profiles are observed respectively. The very minimum occurrences are in the hours of 120 UTC to 180 UTC. This establishes the fact from previous literature that low-level jets are a nocturnal phenomena.

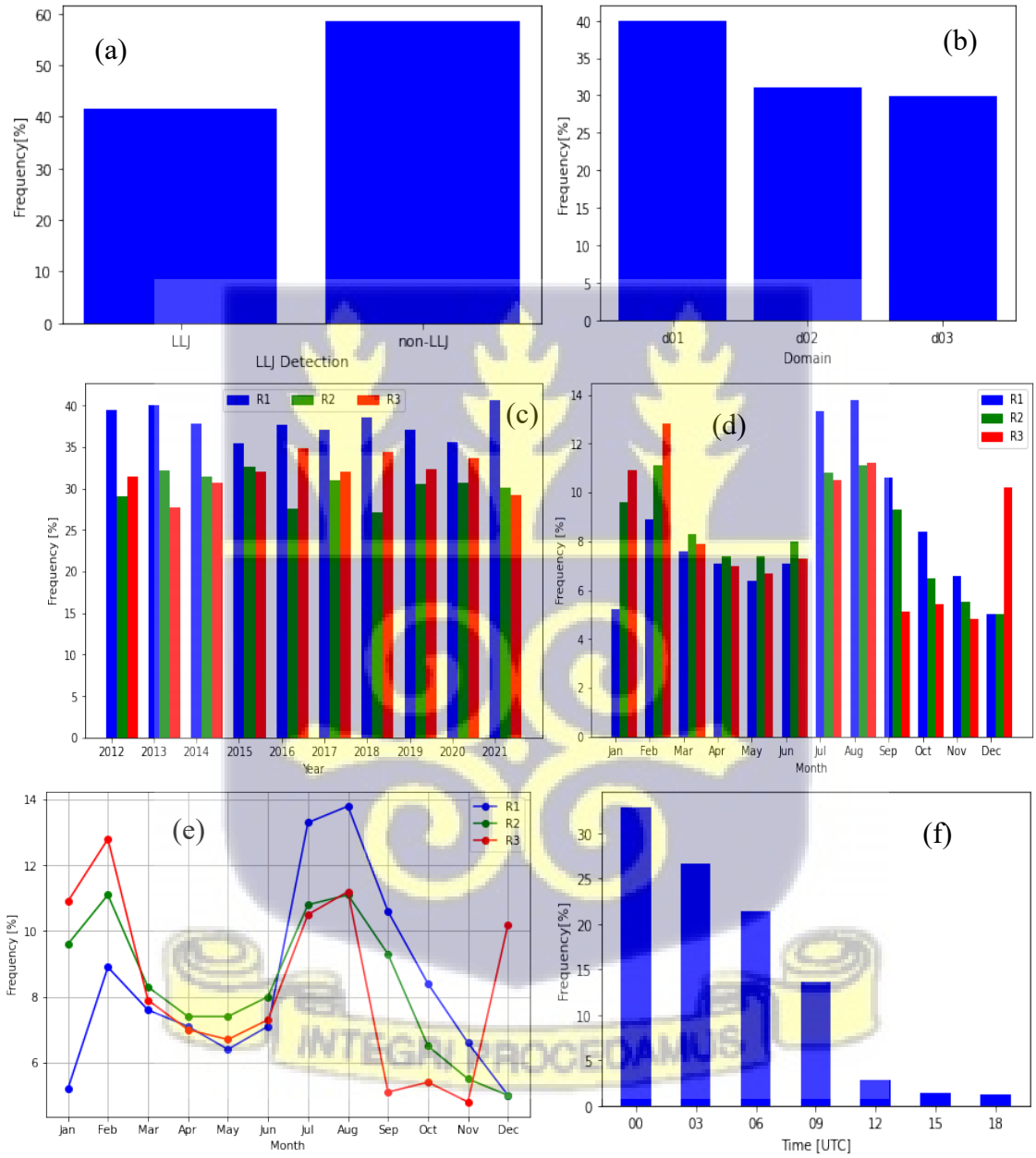

Figure 4.3: Frequency of occurrences of low-level jets over the three bioclimatic regions (R1=Guineo-Congolian Region, R2= Guinean Region , R3=West Sudanian Savanna Region) within southern West-Africa: (a) Bar chart of low-level-jet Detection (b) Bar chart of Domain grouping (c) Bar chart of Yearly grouping (d) Bar chart of Monthly grouping (e) Line chart of Monthly Occurence (f) Time of Occurences.

4.1.3 Height of Occurrence of Low-Level Jets

The study analysed several low-level jet profiles to determine the heights at which low-level jets predominantly occur. Determining the height at which low-level jets occur is important because there is a large significant wind shear just below and above it. Several literature have documented the effects of wind shear on the surface as discussed in Section 2.1. Generally, all detected low-level jets occurred within the height range of 600 – 1000 m (Figure 4.4(b)). Figure 4.4(a) shows that 75% of the low-level jets occur between the heights of 700 – 750 m above ground level. Also, 10% of the low-level jets are observed to occur at 900 – 950 m above ground level. However, at 600 – 650 m height, the frequency of occurrence is 5% and the lowest is 2.5% occuring at 800 – 850 m above ground level. The study observed that low-level jets that occur at 000 UTC – 060 UTC are found in the 700 – 750 m height range. Those that occur at 090UTC – 150 UTC occur at the height range 900 – 950 m. Low-level jets that rarely occur at 180 UTC are found at the height range of 600 – 650 m.

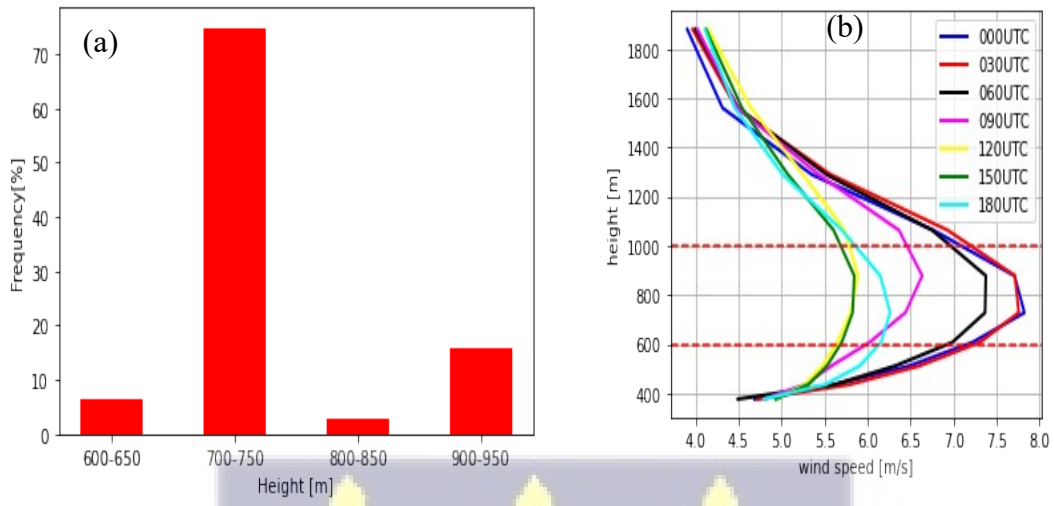

Figure 4.4: Height of Occurrences of low-level jets: (a) Bar chart depicting the frequency vs height of low-level jet occurrence (b) A low-level jet profile for seven (7) different hours observed in August 2020.

4.1.4 Direction of Propagation of Low-level jets

The direction of propagation of low-level jet plays a key role in what low-level jets transport over the surface. In this study, wind rose are visualised over the three (3) regions to ascertain the direction in which low-level jets frequently propagate and the speed for each sampling period. Figure 4.5(a) is a wind rose and a bar chart over R1. The wind rose has two main spokes; a longer spoke and a shorter spoke (Figure 4.5(a)). The longer spoke shows the wind blew from the southwest at speeds between 2.2 - 3.4 m/s (dark blue) about 11.4% of the time, 3.4 – 4.6 m/s (light blue) about 22.7% of the time, 4.6 – 5.8 m/s (light green) about 34.1% of the time, 5.8 – 7.0 m/s (lime green) about 45.4% of the time and 7.0 – 8.1 m/s (orange) about 56.8% of the time. The maximum monthly averaged wind speed observed in R1 is 8.1 m/s. The second spoke shows wind blew from south-southwest at speeds between 5.8 – 7.0 m/s (lime green) about 24% of the time, 4.6 – 5.8 m/s (light green) about 22.7% of the time and 4.4 – 4.6 m/s (light blue) about 17.1%of the time.

However, in Figure 4.5(b) the wind rose have two main spokes and eight (8) small spokes demonstrating the direction and speed of winds at a particular time over R2. The longest spoke illustrates that wind blew from southwest at speeds between 7.5 – 8.9 m/s (orange) about 37.2% of the time, 6.1 – 7.5m/s (lime green) about 26.1% of the time and 4.7 – 6.1m/s (light green) about 23.5% of the time. The second to the longest spoke shows wind blew from south-southwest at speeds between 6.1 – 7.5 m/s (lime green) about 26% of the time and 4.7 – 6.1 m/s (light green) about 28.2% of the time. Four (4) of the smaller spokes show wind blew from south-southeast, east-southeast and east. The maximum monthly averaged wind speed observed in R2 is 8.9 m/s.

Moreover, Figure 4.5(c) is a wind rose with six spokes representing the direction of propagation of low-level jets over R3. The longest spoke shows the wind blew from the east at speeds between 2.5 – 4.6 m/s (light blue) about 9.7% of the time, 4.6 – 6.6 m/s (light green) about 16.9% of the time, 8.7 – 10.8 m/s (lime green) about 22.1% of the time and 10.8 – 12.9 m/s (red) about 24.1% of the time. The second spoke shows the wind blew from the southwest at speeds between 2.5 – 4.6 m/s (dark blue) about 4.8% of the time, 4.6 – 6.6 m/s (blue) about 14.5% of the time, 6.6 – 8.7 m/s (light green) about 20.7% of the time and 8.7–10.8 m/s (lime green) about 21.7% of the time.

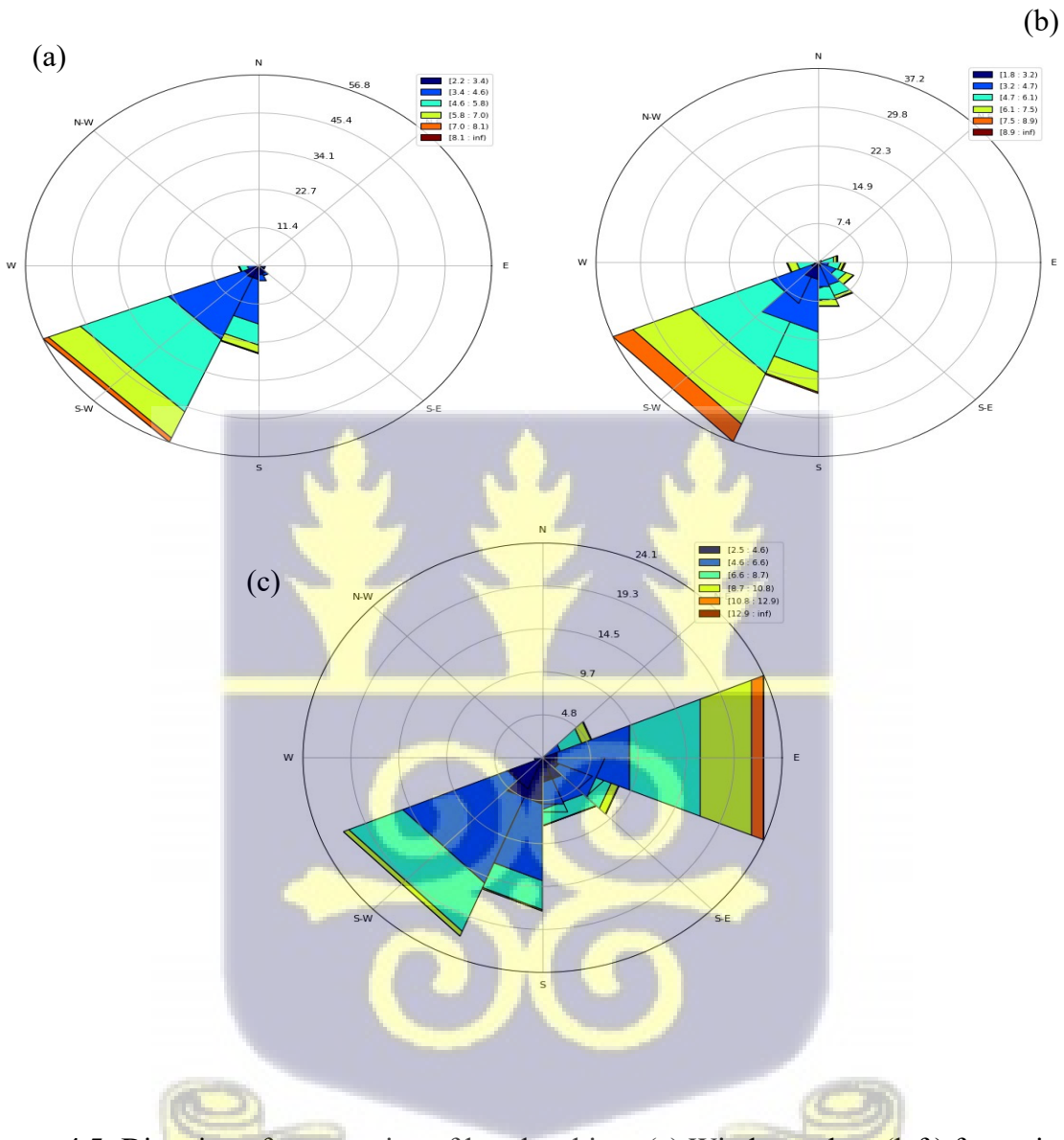

Figure 4.5: Direction of propagation of low-level jets: (a) Windrose chart (left) for region R1, (b) Windrose chart (right) for region R2 and (c) Wind rose (bottom) for region R3

4.2 Discussion of Results

The WRF-model simulation with parameterization schemes: WRF Single Moment -6 class graupel microphysics scheme (Hong and Lim, 2006), Dudhia shortwave radiation scheme (Dudhia, 1989), Mellor-Yamada-Nakanishi-Niino (MYNN) 2.5 level TKE boundary layer scheme (Nakanishi and Niino, 2009), Noah land surface model (Tewari et al., 2004) performed better in the Guineo-Congolian region (R1) which is a coastal area of low terrain elevation with very minimal errors than the West Sudanian Savanna region (R3) and Guinean region (R2), areas with high terrain elevation such as Guinean Highlands and the Jos Plateau in central Nigeria and forest zones. As a result, the 10-year characterization of the frequency of WRF-simulated low-level jet occurrences show that low-level jets are more frequent in the Guineo-Congolian region (R1) than the West Sudanian Savanna region (R3) and Guinean region (R2) in southern West Africa. These results are consistent with several studies predicting low-level jets frequently occurring in coastal regions with strong horizontal temperature gradients (Aird et al., 2021; Ranjha et al., 2013; Tuononen et al.,2015). The frequency of low-level jets over southern West Africa rises twice a year in southern West Africa (Figure 4.3(e)). The first rise in its occurrence is from November to February, with its peak in February, and the second rise is from June to August, with its peak in August, as presented in Section 4.1.2. However, from November to December, the frequency of occurrence of low-level jets is dominant in the West Sudanian Savanna region (R3) and least dominant in the Guineo-Congolian region. In contrast, the frequency of occurrence of low-level jets is dominant in the Guineo-Congolian region from June to August and least dominant in the West Sudanian Savanna region.

This is attributed to the West African Monsoon, which dominates over West Africa from the month of June through the month of September, and the Harmattan flow, which dominates over West Africa from November to mid-March. The reason is low-level jets have are embedded more frequently in either the dry north-easterly Harmattan flow or the south-westerly Monsoon flow, and the orientation is controlled by the position of the Saharan Heat Low (Allen and Washington, 2014). According to Karipot et al. (2009) description of nocturnal low-level jets seen in the North Florida region, low-level jets happen more frequently during the colder months of November to February (70% of the nocturnal periods), as opposed to the warmer months of June to August (47%).

Additionally, during the hours of 000 UTC and 060 UTC, or 12 am and 6 am local time, almost 90% of the low-level jets detected in this study were observed. As mentioned earlier, the findings are consistent with other studies that identified low-level jets as a nighttime phenomenon that occurs between 000 UTC and 060 UTC (Allen and Washington, 2014; Nascimento et al., 2016). Few low-level jets are detected between 090 and 180UTC due to the drag produced by boundary layer turbulence, or more specifically, from the greater turbulent diffusion of momentum, which causes the low-level wind maximum to vanish during the day.

Furthermore, it is worth noting that low-level jets observed frequently occur between the height of 700 – 750 m above ground level, an average of 725 m. This result is consistent with a study on nocturnal low-level clouds over southern West Africa by Adler et al. (2017). Their study observed low-level jets within the height range of 600 – 900 m above ground level, most between 700 – 750 m.

Their study applied COSMO model version 5.1 whiles this study applied WRF model version 4.1.1. Karipot et al. (2009) also observed low- level jets occur at the heights between 80 and 700 m over North Florida area. Ruchith and Ernest Raj (2015) worked on features of nocturnal low-level jet observed over a tropical Indian station using high resolution Doppler wind lidar.

They observed most low-level jets occurring in the 600 – 700 m height above ground level. Besides, within the three bioclimatic regions, most low-level jets propagate from the southwest direction in the Guineo-Congolian region (R1) with a maximum average speed of 8.1 m/s. In the Guinean region (R1), most low-level jets propagate from the southwest direction. In contrast, low-level jets observed over the West Sudanian Savanna region(R3) mainly propagate eastward with a mean low-level jet maximum (jet core) of 12.9 m/s. Also, in the Guinean region (R2), most low-level jets propagate south-westerly with a mean low-level jet maximum (jet core) of 8.9 m/s. In other literature, Ranjha et al. (2013) documented that the most commonly found coastal low-level jets have a maximum wind speed between 9 and 15 m/s and occur at heights between 500 and 700 m above ground level. Aird et al. (2021) demonstrated that low-level jets have a spatiotemporal mean wind speed maximum of 9.55 m/s.

CHAPTER FIVE

CONCLUSION AND RECOMMENDATIONS

5.1 Conclusion

High-resolution WRF simulations over southern West Africa from January 2012 to December 2021 are analysed to generate seasonal analysis on low-level jets. Low-level jet characteristics include frequency, intensity, height of occurrence, and propagation direction. Three bioclimatic areas found in southern West Africa were used as the basis for the analysis. West Sudanian Savanna, Guinean region, and Guineo Congolian region are the bioclimatic regions considered.

The study, using a detection algorithm, observed that low-level jets frequently occur in the Guineo Congolian region of southern West Africa and mainly propagates from the southwest with a maximum wind speed of 8.1 m/s. According to Holton (1967), the horizontal variations in latent heat flux and sensible heat flux produce strong low-level baroclinicity, which is the cause of the low-level jets seen in the Guineo Congolian region (Holton, 1967). Besides, low-level jets detected in the Guinean region occur the least frequently compared to the other two regions. These jets propagate from the southwest and have a maximum jet core speed of 8.9 m/s. Since the topography in this area ranges from coastal plains to inland mountains, low-level baroclinicity formed as a result of sea-land surface characteristics and low-level baroclinicity formed as a result of sloping terrain can both be attributed to the formation of these low-level jets in this region. However, the frequency of low-level jets observed in the West Sudanian Savanna region is second to the Guineo-Congolian region. With a maximum average wind speed of 12.9 m/s, the low-level jets in this region are observed to propagate from the east from November to February and from the southwest

from March to October. Since it has been demonstrated by Karipot et al. (2009) that low-level jets over West Africa are embedded in Harmattan winds or Monsoon winds, the reason for the propagation from the east from the indicated time is due to the intensification of the Harmattan winds from November to February.

The increase in low-level jet wind speed maximum in the West Sudanian Savanna region compared to the low-level jet wind speeds for the other regions may be due to a greater forcing contribution from Blackadar mechanism (Blackadar, 1957). Generally, the detected low-level jets occur between the hours of 000 UTC – 060 UTC for the entire southern West Africa at an average height of 725 m.

5.2 Recommendations

Based on the conclusions made, low-level jets with typical intensity and mesoscale characteristics may be frequent over southern West Africa during the warm season. Stakeholders should expect increasingly precise predictions of low-level jet occurrences from the current real-time forecasts and operational models in many circumstances as model initial conditions and physical parameterizations continue to improve. The intensity, orientation, and position of low-level jets, as well as the spatial and diurnal changes of lower tropospheric flows, are all significantly influenced by surface heat fluxes, land-ocean contrasts, inland mountains, and forests. To apply the aforementioned conclusions to both warm and cold seasons in southern West Africa, more observational and modelling case studies are required. However, as the research outlines how frequent LLJs occurs in various months of the year, it would serve as a needful tool for aviation policymakers and air traffic safety researchers since LLJs are associated with wind shears. In addition, it would serve as a useful tool to

local meteorological stations in regions within the study area for weather forecasting and observations.

REFERENCES

Adler, B., Kalthoff, N., & Gantner, L. (2017). Nocturnal low-level clouds over southern West Africa analysed using high-resolution simulations. *Atmospheric Chemistry and Physics*, 17(2), 899–910. https://doi.org/10.5194/acp-17-899-2017

Aird, J. A., Barthelmie, R. J., Shepherd, T. J., & Pryor, S. C. (2021). WRF-simulated low-level jets over Iowa: Characterization and sensitivity studies. *Wind Energy Science*, 6(4), 1015–1030. https://doi.org/10.5194/wes-6-1015-2021

Algarra, I., Eiras-Barca, J., Nieto, R., & Gimeno, L. (2019). Global climatology of nocturnal low-level jets and associated moisture sources and sinks. *Atmospheric Research*, 229, 39–59. https://doi.org/10.1016/j.atmosres.2019.06.016

Allen, C. J. T., & Washington, R. (2014). The low-level jet dust emission mechanism in the central Sahara: Observations from Bordj-Badji Mokhtar during the June 2011 Fennec Intensive Observation Period. *Journal of Geophysical Research: Atmospheres*, 119(6), 2990–3015. https://doi.org/10.1002/2013JD020594

Andreas, E. L., Claffy, K. J., & Makshtas, A. P. (2000). Low-level atmospheric jets and inversions over the western Weddell Sea. *Boundary-Layer Meteorology*, 97(3), 459–486.

Arritt, R. W., Rink, T. D., Segal, M., Todey, D. P., Clark, C. A., Mitchell, M. J., & Labas, K. M. (1997a). The Great Plains low-level jet during the warm season of 1993. *Monthly Weather Review*, 125(9), 2176–2192.

Arritt, R. W., Rink, T. D., Segal, M., Todey, D. P., Clark, C. A., Mitchell, M. J., & Labas, K. M. (1997b). The Great Plains Low-Level Jet during the Warm Season of 1993.

Monthly Weather Review, 125(9), 2176–2192. https://doi.org/10.1175/1520-0493(1997)125<2176:TGPLLJ>2.0.CO;2

Baas, P., Bosveld, F. C., Klein Baltink, H., & Holtslag, A. A. M. (2009). A climatology of nocturnal low-level jets at Cabauw. *Journal of Applied Meteorology and Climatology*, 48(8), 1627–1642.

Banta, R. M., Newsom, R. K., Lundquist, J. K., Pichugina, Y. L., Coulter, R. L., & Mahrt, L. (2002). Nocturnal Low-Level Jet Characteristics Over Kansas During Cases-99. *Boundary-Layer Meteorology*, 105(2), 221–252. https://doi.org/10.1023/A:1019992330866

Beebe, R. G., & Bates, F. C. (1955). A MECHANISM FOR ASSISTING IN THE RELEASE OF CONVECTIVE INSTABILITY. *Monthly Weather Review*, 83(1), 1–10. https://doi.org/10.1175/1520-0493(1955)083<0001:AMFAIT>2.0.CO;2

Bentley, M. L., & Mote, T. L. (1998). A Climatology of Derecho-Producing Mesoscale Convective Systems in the Central and Eastern United States, 1986–95. Part I: Temporal and Spatial Distribution. *Bulletin of the American Meteorological Society*, 79(11), 2527–2540. https://doi.org/10.1175/1520-0477(1998)079<2527:ACODPM>2.0.CO;2

Blackadar, A. K. (1957). Boundary Layer Wind Maxima and Their Significance for the Growth of Nocturnal Inversions. *Bulletin of the American Meteorological Society*, 38(5), 283–290. https://doi.org/10.1175/1520-0477-38.5.283

Bonner, W. D. (1968). Climatology of the Low-level jet. *Monthly Weather Review*, 96(12), 833–850. https://doi.org/10.1175/1520-0493(1968)096<0833:COTLLJ>2.0.CO;2

Bonner, W. D., & Paegle, J. (1970). Diurnal Variations in Boundary Layer Winds over the South-Central United States in Summer. *Monthly Weather Review*, 98(10), 735–744. https://doi.org/10.1175/1520-0493(1970)098<0735:DVIBLW>2.3.CO;2

Bosart, L. F., & Sanders, F. (1981). The Johnstown Flood of July 1977: A Long-Lived Convective System. *Journal of the Atmospheric Sciences*, 38(8), 1616–1642. https://doi.org/10.1175/1520-0469(1981)038<1616:TJFOJA>2.0.CO;2

Buajitti, K., & Blackadar, A. K. (1957). Theoretical studies of diurnal wind-structure variations in the planetary boundary layer. *Quarterly Journal of the Royal Meteorological Society*, 83(358), 486–500. https://doi.org/10.1002/qj.49708335804

Carpman, N. (2011). *Turbulence Intensity in Complex Environments and its Influence on Small Wind Turbines*. http://urn.kb.se/resolve?urn=urn:nbn:se:uu:diva-153215

Charney, J. G. (1955). The gulf stream as an inertial boundary layer. *Proceedings of the National Academy of Sciences*, 41(10), 731–740. https://doi.org/10.1073/pnas.41.10.731

Chen, Y.-L., Chen, X. A., & Zhang, Y.-X. (1994). A Diagnostic Study of the Low-Level Jet during TAMEX IOP 5. *Monthly Weather Review*, 122(10), 2257–2284. https://doi.org/10.1175/1520-0493(1994)122<2257:ADSOTL>2.0.CO;2

Cook, K. H., Vizy, E. K., Launer, Z. S., & Patricola, C. M. (2008). Springtime intensification of the Great Plains low-level jet and Midwest precipitation in GCM simulations of the twenty-first century. *Journal of Climate*, 21(23), 6321–6340.

Cotillon, S. E., & Tappan, G. G. (2016). Landscapes of West Africa: A window on a changing world.

Crawford, K. C., & Hudson, H. R. (1970). *Behavior of Winds in the Lowest 1500 Feet in Central Oklahoma: June, 1966-May, 1967*. National Severe Storms Laboratory.

Djurić, D., & Damiani, M. S. (1980). On the Formation of the Low-Level Jet over Texas. *Monthly Weather Review*, 108(11), 1854–1865. https://doi.org/10.1175/1520-0493(1980)108<1854:OTFOTL>2.0.CO;2

Douglas, M. W. (1995). The Summertime Low-Level Jet over the Gulf of California. *Monthly Weather Review*, 123(8), 2334–2347. https://doi.org/10.1175/1520-0493(1995)123<2334:TSLLJO>2.0.CO;2

Doyle, J. D., & Warner, T. T. (1991). A Carolina Coastal Low-Level Jet during GALE IOP 2. *Monthly Weather Review*, 119(10), 2414–2428. https://doi.org/10.1175/1520-0493(1991)119<2414:ACCLLJ>2.0.CO;2

Du, Y., Zhang, Q., Chen, Y., Zhao, Y., & Wang, X. (2014). Numerical Simulations of Spatial Distributions and Diurnal Variations of Low-Level Jets in China during Early Summer. *Journal of Climate*, 27(15), 5747–5767. https://doi.org/10.1175/JCLI-D-13-00571.1

Du, Y., Zhang, Q., Ying, Y., & Yang, Y. (2012). Characteristics of Low-level Jets in Shanghai during the 2008-2009 Warm Seasons as Inferred from Wind Profiler Radar Data. *Meteorological Journal.*, 90(6), 891–903. https://doi.org/10.2151/jmsj.2012-603

Dudhia, J. (1989). Numerical Study of Convection Observed during the Winter Monsoon Experiment Using a Mesoscale Two-Dimensional Model. *Journal of the Atmospheric Sciences*, 46(20), 3077–3107. https://doi.org/10.1175/1520-0469(1989)046<3077:NSOCOD>2.0.CO;2

Dzebre, D. E. K., Acheampong, A. A., Ampofo, J., & Adaramola, M. S. (2019). A sensitivity study of Surface Wind simulations over Coastal Ghana to selected Time Control and Nudging options in the Weather Research and Forecasting Model. *Heliyon*, 5(3), e01385. https://doi.org/10.1016/j.heliyon.2019.e01385

Enfield, D. B. (1981). Thermally driven wind variability in the planetary boundary layer above Lima, Peru. *Journal of Geophysical Research: Oceans*, 86(C3), 2005–2016. https://doi.org/10.1029/JC086iC03p02005

Farquharson, J. S. (1939). The diurnal variation of wind over tropical Africa. *Quarterly Journal of the Royal Meteorological Society*, 65(280), 165–184. https://doi.org/10.1002/qj.49706528004

Fiedler, S., Schepanski, K., Heinold, B., Knippertz, P., & Tegen, I. (2013). Climatology of nocturnal low-level jets over North Africa and implications for modeling mineral dust emission. *Journal of Geophysical Research: Atmospheres*, 118(12), 6100–6121. https://doi.org/10.1002/jgrd.50394

Forbes, G. S., Thomson, D. W., & Anthes, R. A. (1987). Synoptic and Mesoscale Aspects of an Appalachian Ice Storm Associated with Cold-Air Damming. *Monthly Weather Review*, 115(2), 564–591. https://doi.org/10.1175/1520-0493(1987)115<0564:SAMAOA>2.0.CO;2

Frisch, A. S., Orr, B. W., & Martner, B. E. (1992). Doppler Radar Observations of the Development of a Boundary-Layer Nocturnal Jet. *Monthly Weather Review*, 120(1), 3–16. https://doi.org/10.1175/1520-0493(1992)120<0003:DROOTD>2.0.CO;2

Gevorgyan, A. (2018). A Case Study of Low-Level Jets in Yerevan Simulated by the WRF Model. *Journal of Geophysical Research: Atmospheres*, 123(1), 300–314. https://doi.org/10.1002/2017JD027629

Gimeno, Luis, Francina Dominguez, Raquel Nieto, Ricardo Trigo, Anita Drumond, Chris JC Reason, Andréa S. Taschetto, Alexandre M. Ramos, Ramesh Kumar, and José Marengo. "Major mechanisms of atmospheric moisture transport and their role in extreme precipitation events." *Annual Review of Environment and Resources* 41 (2016): 117-141.

Grell, G. A., & Dévényi, D. (2002). A generalized approach to parameterizing convection combining ensemble and data assimilation techniques. *Geophysical Research Letters*, 29(14), 38-1-38–4. https://doi.org/10.1029/2002GL015311

Helfand, H. M., & Schubert, S. D. (1995). Climatology of the simulated Great Plains low-level jet and its contribution to the continental moisture budget of the United States. *Journal of Climate*, 8(4), 784–806.

Higgins, R. W., Yao, Y., & Wang, X. L. (1997). Influence of the North American Monsoon System on the U.S. Summer Precipitation Regime. *Journal of Climate*, 10(10), 2600–2622. https://doi.org/10.1175/1520-0442(1997)010<2600:IOTNAM>2.0.CO;2

Hoecker, W. H. (1963). Three Southerly Low-level Jet System Delineated by the Weather Bureau Special Pibal Network of 1961. *Monthly Weather Review*, 91(10), 573–582. https://doi.org/10.1175/1520-0493(1963)091<0573:TSLJSD>2.3.CO;2

Højberg, A. L., & Refsgaard, J. C. (2005). Model uncertainty–parameter uncertainty versus conceptual models. *Water Science and Technology*, *52*(6), 177-186.

Holton, J. R. (1967). The diurnal boundary layer wind oscillation above sloping terrain. *Tellus*, 19(2), 200–205. https://doi.org/10.3402/tellusa.v19i2.9766

Hong, S.-Y., & Lim, J.-O. J. (2006). The WRF single-moment 6-class microphysics scheme (WSM6). *Asia-Pacific Journal of Atmospheric Sciences*, 42(2), 129–151.

Hoxit, L. R. (1975). Diurnal variations in planetary boundary-layer winds over land. *Boundary-Layer Meteorology*, 8(1), 21–38.

Hu, X.-M., Klein, P. M., & Xue, M. (2013). Evaluation of the updated YSU planetary boundary layer scheme within WRF for wind resource and air quality assessments. *Journal of Geophysical Research: Atmospheres*, 118(18), 10,490-10,505. https://doi.org/10.1002/jgrd.50823

Jiang, X., Lau, N.-C., Held, I. M., & Ploshay, J. J. (2007a). Mechanisms of the Great Plains low-level jet as simulated in an AGCM. *Journal of the Atmospheric Sciences*, 64(2), 532–547.

Jiang, X., Lau, N.-C., Held, I. M., & Ploshay, J. J. (2007b). Mechanisms of the Great Plains Low-Level Jet as Simulated in an AGCM. *Journal of the Atmospheric Sciences*, 64(2), 532–547. https://doi.org/10.1175/JAS3847.1

Jiménez-Sánchez, G., Markowski, P. M., Jewtoukoff, V., Young, G. S., & Stensrud, D. J. (2019). The Orinoco Low-Level Jet: An Investigation of Its Characteristics and Evolution Using the WRF Model. *Journal of Geophysical Research: Atmospheres*, 124(20), 10696–10711. https://doi.org/10.1029/2019JD030934

Ju, T., Wu, B., Wang, Z., Liu, J., Chen, D., & Zhang, H. (2020). Relationships between Low-Level Jet and Low Visibility Associated with Precipitation, Air Pollution, and Fog in Tianjin. *Atmosphere*, 11(11), 11. https://doi.org/10.3390/atmos11111197

Karipot, A., Leclerc, M. Y., & Zhang, G. (2009). Characteristics of Nocturnal Low-Level Jets Observed in the North Florida Area. *Monthly Weather Review*, 137(8), 2605–2621. https://doi.org/10.1175/2009MWR2705.1

Kato, T. (1998). Numerical Simulation of the Band-shaped Torrential Rain Observed over Southern Kyushu, Japan on 1 August 1993. *Journal of the Meteorological Society of Japan. Ser. II*, 76(1), 97–128. https://doi.org/10.2151/jmsj1965.76.1_97

Knippertz, P. (2008). Dust emissions in the West African heat trough the role of the diurnal cycle and of extratropical disturbances. *Meteorologische Zeitschrift*, 17(5), 553–563. https://doi.org/10.1127/0941-2948/2008/0315

Lewis, C.D. (1982). Industrial and business forecasting methods. London: Butterworths.

Lothon, M., Saïd, F., Lohou, F., & Campistron, B. (2008). Observation of the Diurnal Cycle in the Low Troposphere of West Africa. *Monthly Weather Review*, 136(9), 3477–3500. https://doi.org/10.1175/2008MWR2427.1

Maddox, R. A. (1983). Large-Scale Meteorological Conditions Associated with Midlatitude, Mesoscale Convective Complexes. *Monthly Weather Review*, 111(7), 1475–1493. https://doi.org/10.1175/1520-0493(1983)111<1475:LSMCAW>2.0.CO;2

Mahrt, L. (1981). The early evening boundary layer transition. *Quarterly Journal of the Royal Meteorological Society*, 107(452), 329–343. https://doi.org/10.1002/qj.49710745205

Marengo, J. A., Soares, W. R., Saulo, C., & Nicolini, M. (2004). Climatology of the Low-Level Jet East of the Andes as Derived from the NCEP–NCAR Reanalyses: Characteristics and Temporal Variability. *Journal of Climate*, 17(12), 2261–2280. https://doi.org/10.1175/1520-0442(2004)017<2261:COTLJE>2.0.CO;2

Markowski, P., & Richardson, Y. (2011). *Mesoscale meteorology in midlatitudes* (Vol. 2). John Wiley & Sons.

Mccorcle, M. D. (1988). Simulation of surface-moisture effects on the Great Plains low-level jet. *Monthly Weather Review*, 116(9), 1705–1720.

McMillan, H. K., Westerberg, I. K., & Krueger, T. (2018). Hydrological data uncertainty and its implications. *Wiley Interdisciplinary Reviews: Water*, *5*(6), e1319.

McNider, R. T., & Pielke, R. A. (1981). Diurnal Boundary-Layer Development over Sloping Terrain. *Journal of the Atmospheric Sciences*, 38(10), 2198–2212. https://doi.org/10.1175/1520-0469(1981)038<2198:DBLDOS>2.0.CO;2

Means, L. L. (1954a). A Study of the Mean Southerly Wind-Maximum in Low Levels Associated with a Period of Summer Precipitation in the Middle West. *Bulletin of the American Meteorological Society*, 35(4), 166–170. https://doi.org/10.1175/1520-0477-35.4.166

Means, L. L. (1954b). A Study of the Mean Southerly Wind-Maximum in Low Levels Associated with a Period of Summer Precipitation in the Middle West. *Bulletin of the American Meteorological Society*, 35(4), 166–170. https://doi.org/10.1175/1520-0477-35.4.166

Mitchell, M. J., Arritt, R. W., & Labas, K. (1995). A Climatology of the Warm Season Great Plains Low-Level Jet Using Wind Profiler Observations. *Weather and Forecasting*, 10(3), 576–591. https://doi.org/10.1175/1520-0434(1995)010<0576:ACOTWS>2.0.CO;2

Mlawer, E. J., Taubman, S. J., Brown, P. D., Iacono, M. J., & Clough, S. A. (1997). Radiative transfer for inhomogeneous atmospheres: RRTM, a validated correlated-k model for the longwave. *Journal of Geophysical Research: Atmospheres*, 102(D14), 16663–16682. https://doi.org/10.1029/97JD00237

Munday, C., Washington, R., & Hart, N. (2021). African Low-Level Jets and Their Importance for Water Vapor Transport and Rainfall. *Geophysical Research Letters*, 48(1), e2020GL090999. https://doi.org/10.1029/2020GL090999

Nakanishi, M., & Niino, H. (2009). Development of an Improved Turbulence Closure Model for the Atmospheric Boundary Layer. *Meteorology Journal Volume 2*, 87(5), 895–912. https://doi.org/10.2151/jmsj.87.895

Nascimento, M. G. do, Herdies, D. L., & Souza, D. O. de. (2016). The South American Water Balance: The Influence of Low-Level Jets. *Journal of Climate*, 29(4), 1429–1449. https://doi.org/10.1175/JCLI-D-15-0065.1

Nicolini, M., Waldron, K. M., & Paegle, J. (1993). Diurnal Oscillations of Low-Level Jets, Vertical Motion, and Precipitation: A Model Case Study. *Monthly Weather Review*, 121(9), 2588–2610. https://doi.org/10.1175/1520-0493(1993)121<2588:DOOLLJ>2.0.CO;2

Paegle, J., & McLAWHORN, D. W. (1973). Correlation of Nocturnal Thunderstorms and Boundary-Layer Convergence. *Monthly Weather Review*, 101(12), 877–883. https://doi.org/10.1175/1520-0493(1973)101<0877:CONTAB>2.3.CO;2

Paegle, J., & Rasch, G. E. (1973). Three-Dimensional Characteristics of Diurnally Varying Boundary-Layer Flows. *Monthly Weather Review*, 101(10), 746–756. https://doi.org/10.1175/1520-0493(1973)101<0746:TCODVB>2.3.CO;2

Pamperin, H., & Stilke, G. (1985). Nächtliche Grenzschicht und LLJ im Alpenvorland nahe dem Inntalausgang. *Meteorologische Rundschau*, 38(5), 145–156.

Parish, T. R. (2000). Forcing of the Summertime Low-Level Jet along the California Coast. *Journal of Applied Meteorology and Climatology*, 39(12), 2421–2433. https://doi.org/10.1175/1520-0450(2000)039<2421:FOTSLL>2.0.CO;2

Parish, T. R., & Oolman, L. D. (2010a). On the role of sloping terrain in the forcing of the Great Plains low-level jet. *Journal of the Atmospheric Sciences*, 67(8), 2690–2699.

Parish, T. R., & Oolman, L. D. (2010b). On the Role of Sloping Terrain in the Forcing of the Great Plains Low-Level Jet. *Journal of the Atmospheric Sciences*, 67(8), 2690–2699. https://doi.org/10.1175/2010JAS3368.1

Parish, T. R., Rodi, A. R., & Clark, R. D. (1988). A Case Study of the Summertime Great Plains Low Level Jet. *Monthly Weather Review*, 116(1), 94–105. https://doi.org/10.1175/1520-0493(1988)116<0094:ACSOTS>2.0.CO;2

Pham, N. T., Nakamura, K., Furuzawa, F. A., & Satoh, S. (2008). Characteristics of Low Level Jets over Okinawa in the Baiu and post-Baiu Seasons Revealed by Wind Profiler Observations. *Meteorology Journal Volume 2*, 86(5), 699–717. https://doi.org/10.2151/jmsj.86.699

Porter, J. M., Means, L. L., Hovde, J. E., & Chappell, W. B. (1955). A Synoptic Study on the Formation of Squall Lines in the North Central United States. *Bulletin of the American Meteorological Society*, 36(8), 390–396. https://doi.org/10.1175/1520-0477-36.8.390

Ranjha, R., Svensson, G., Tjernström, M., & Semedo, A. (2013). Global distribution and seasonal variability of coastal low-level jets derived from ERA-Interim reanalysis. *Tellus A: Dynamic Meteorology and Oceanography*, 65(1), 20412. https://doi.org/10.3402/tellusa.v65i0.20412

Reiter, E. R. (1963). *Jet-stream meteorology*. University of Chicago Press.

Reiter, E. R., & Whitney, L. F. (1969). Interaction BETWEEN SUBTROPICAL AND POLAR-FRONT JET STREAM. *Monthly Weather Review*, 97(6), 432–438. https://doi.org/10.1175/1520-0493(1969)097<0432:IBSAPJ>2.3.CO;2

Rife, D. L., Pinto, J. O., Monaghan, A. J., Davis, C. A., & Hannan, J. R. (2010a). Global Distribution and Characteristics of Diurnally Varying Low-Level Jets. *Journal of Climate*, 23(19), 5041–5064. https://doi.org/10.1175/2010JCLI3514.1

Rife, D. L., Pinto, J. O., Monaghan, A. J., Davis, C. A., & Hannan, J. R. (2010b). Global Distribution and Characteristics of Diurnally Varying Low-Level Jets. *Journal of Climate*, 23(19), 5041–5064. https://doi.org/10.1175/2010JCLI3514.1

Rojas, R., Feyen, L., & Dassargues, A. (2008). Conceptual model uncertainty in groundwater modeling: Combining generalized likelihood uncertainty estimation and Bayesian model averaging. *Water Resources Research*, *44*(12).

Ruchith, R. D., & Ernest Raj, P. (2015). Features of nocturnal low level jet (NLLJ) observed over a tropical Indian station using high resolution Doppler wind lidar. *Journal of Atmospheric and Solar-Terrestrial Physics*, 123, 113–123. https://doi.org/10.1016/j.jastp.2015.01.001

Samman, A. E., & Gallus Jr., W. A. (2018). A climatology of the winter low-level jet over the Red Sea. *International Journal of Climatology*, 38(15), 5505–5521. https://doi.org/10.1002/joc.5742

Slättberg, N. (2020). *Planetary Boundary Layer Height Variations Over the Tibetan Plateau in Relation to Local Climate Variables and Large-Scale Circulation*. https://gupea.ub.gu.se/handle/2077/66396

Smith, E. N., Gibbs, J. A., Fedorovich, E., & Klein, P. M. (2018). WRF Model Study of the Great Plains Low-Level Jet: Effects of Grid Spacing and Boundary Layer Parameterization. *Journal of Applied Meteorology and Climatology*, 57(10), 2375–2397. https://doi.org/10.1175/JAMC-D-17-0361.1

Soares, P. M. M., Cardoso, R. M., Semedo, Ál., Chinita, M. J., & Ranjha, R. (2014). Climatology of the Iberia coastal low-level wind jet: Weather research forecasting model high-resolution results. *Tellus A: Dynamic Meteorology and Oceanography*, 66(1), 22377. https://doi.org/10.3402/tellusa.v66.22377

Stensrud, D. J. (1996). Importance of Low-Level Jets to Climate: A Review. *Journal of Climate*, 9(8), 1698–1711.

Storm, B., Dudhia, J., Basu, S., Swift, A., & Giammanco, I. (2009). Evaluation of the Weather Research and Forecasting model on forecasting low-level jets: Implications for wind energy. *Wind Energy*, 12(1), 81–90. https://doi.org/10.1002/we.288

Sullivan, J. T., Rabenhorst, S. D., Dreessen, J., McGee, T. J., Delgado, R., Twigg, L., & Sumnicht, G. (2017). Lidar observations revealing transport of O3 in the presence of a nocturnal low-level jet: Regional implications for "next-day" pollution. *Atmospheric Environment*, *158*, 160–171. https://doi.org/10.1016/j.atmosenv.2017.03.039

Tay, K., Koh, T.-Y., & Skote, M. (2021). Characterizing mesoscale variability in low-level jet simulations for CBLAST-LOW 2001 campaign. *Meteorology and Atmospheric Physics*, 133(2), 163–179. https://doi.org/10.1007/s00703-020-00736-3

Tepper, M. (1954). *Pressure jump lines in Midwestern United States, January-August 1951* (Vol. 30). US Department of Commerce, Weather Bureau.

Tewari, M., Chen, F., Wang, W., Dudhia, J., LeMone, M. A., Mitchell, K., Ek, M., Gayno, G., Wegiel, J., & Cuenca, R. H. (2004). Implementation and verification of the unified NOAH land surface model in the WRF model. *20th Conference on Weather Analysis and Forecasting/16th Conference on Numerical Weather Prediction*, 1115(6), 2165–2170.

Tuononen, M., Sinclair, V. A., & Vihma, T. (2015). A climatology of low-level jets in the mid-latitudes and polar regions of the Northern Hemisphere. *Atmospheric Science Letters*, 16(4), 492–499. https://doi.org/10.1002/asl.587

Uccellini, L. W., & Johnson, D. R. (1979). The Coupling of Upper and Lower Tropospheric Jet Streaks and Implications for the Development of Severe Convective Storms. *Monthly Weather Review*, 107(6), 682–703. https://doi.org/10.1175/1520-0493(1979)107<0682:TCOUAL>2.0.CO;2

Uccellini, L. W., & Kocin, P. J. (1987). The Interaction of Jet Streak Circulations during Heavy Snow Events along the East Coast of the United States. *Weather and Forecasting*, 2(4), 289–308. https://doi.org/10.1175/1520-0434(1987)002<0289:TIOJSC>2.0.CO;2

Udina, M., Soler, M. R., Olid, M., Jiménez-Esteve, B., & Bech, J. (2020). Pollutant vertical mixing in the nocturnal boundary layer enhanced by density currents and low-level jets: Two representative case studies. *Boundary-Layer Meteorology*, 174(2), 203–230.

Vera, C., Baez, J., Douglas, M., Emmanuel, C. B., Marengo, J., Meitin, J., Nicolini, M., Nogues-Paegle, J., Paegle, J., Penalba, O., Salio, P., Saulo, C., Dias, M. A. S., Dias, P. S., & Zipser, E. (2006). The South American Low-Level Jet Experiment. *Bulletin of the American Meteorological Society*, 87(1), 63–78. https://doi.org/10.1175/BAMS-87-1-63

Veronis, G. (1956). Partition of energy between geostrophic and non-geostrophic oceanic motions. *Deep Sea Research (1953)*, 3(3), 157–177. https://doi.org/10.1016/0146-6313(56)90001-6

Wallace, J. M. (1975). Diurnal Variations in Precipitation and Thunderstorm Frequency over the Conterminous United States. *Monthly Weather Review*, 103(5), 406–419. https://doi.org/10.1175/1520-0493(1975)103<0406:DVIPAT>2.0.CO;2

Walter, B. A., & Overland, J. E. (1984). Observations of Longitudinal Rolls in a Near Neutral Atmosphere. *Monthly Weather Review*, 112(1), 200–208. https://doi.org/10.1175/1520-0493(1984)112<0200:OOLRIA>2.0.CO;2

Werth, D., Kurzeja, R., Dias, N. L., Zhang, G., Duarte, H., Fischer, M., Parker, M., & Leclerc, M. (2011). The Simulation of the Southern Great Plains Nocturnal Boundary Layer and the Low-Level Jet with a High-Resolution Mesoscale Atmospheric Model. *Journal of Applied Meteorology and Climatology*, 50(7), 1497–1513. https://doi.org/10.1175/2011JAMC2272.1

Wexler, H. (1961). A Boundary Layer Interpretation of the Low-level Jet. *Tellus*, 13(3), 368–378. https://doi.org/10.1111/j.2153-3490.1961.tb00098.x

Whiteman, C. D., Bian, X., & Zhong, S. (1997). Low-Level Jet Climatology from Enhanced Rawinsonde Observations at a Site in the Southern Great Plains. *Journal of Applied Meteorology and Climatology*, 36(10), 1363–1376. https://doi.org/10.1175/1520-0450(1997)036<1363:LLJCFE>2.0.CO;2

Wiel, B. J. H. V. de, Moene, A. F., Steeneveld, G. J., Baas, P., Bosveld, F. C., & Holtslag, A. a. M. (2010). A Conceptual View on Inertial Oscillations and Nocturnal Low-Level Jets. *Journal of the Atmospheric Sciences*, 67(8), 2679–2689. https://doi.org/10.1175/2010JAS3289.1

Wu, B., Li, Z., Ju, T., & Zhang, H. (2020a). Characteristics of Low-level jets during 2015–2016 and the effect on fog in Tianjin. *Atmospheric Research*, 245, 105102. https://doi.org/10.1016/j.atmosres.2020.105102

Wu, B., Li, Z., Ju, T., & Zhang, H. (2020b). Characteristics of Low-level jets during 2015–2016 and the effect on fog in Tianjin. *Atmospheric Research*, 245, 105102. https://doi.org/10.1016/j.atmosres.2020.105102

Zemba, J., & Friehe, C. A. (1987). The marine atmospheric boundary layer jet in the Coastal Ocean Dynamics Experiment. *Journal of Geophysical Research: Oceans*, 92(C2), 1489–1496. https://doi.org/10.1029/JC092iC02p01489

Zhang, D.-L., & Fritsch, J. M. (1986). A Case Study of the Sensitivity of Numerical Simulation of Mesoscale Convective Systems to Varying Initial Conditions. *Monthly Weather Review*, 114(12), 2418–2431. https://doi.org/10.1175/1520-0493(1986)114<2418:ACSOTS>2.0.CO;2

Zhang, D.-L., Zhang, S., & Weaver, S. J. (2006). Low-Level Jets over the Mid-Atlantic States: Warm-Season Climatology and a Case Study. *Journal of Applied Meteorology and Climatology*, 45(1), 194–209. https://doi.org/10.1175/JAM2313.1

Zhang, M., & Meng, Z. (2019). Warm-Sector Heavy Rainfall in Southern China and Its WRF Simulation Evaluation: A Low-Level-Jet Perspective. *Monthly Weather Review*, 147(12), 4461–4480. https://doi.org/10.1175/MWR-D-19-0110.1

Zhong, S., Fast, J. D., & Bian, X. (1996). A Case Study of the Great Plains Low-Level Jet Using Wind Profiler Network Data and a High-Resolution Mesoscale Model. *Monthly Weather Review*, 124(5), 785–806. https://doi.org/10.1175/1520-0493(1996)124<0785:ACSOTG>2.0.CO;2